



THE UNIVERSITY *of* EDINBURGH
School of Physics
and Astronomy

Determining the three-gluon Central-emission Vertex at tree-level

MPhys Project Report

D R R Miller

Submitted for the 40pt MPhys Project course PHYS11016
August 28, 2023

Abstract

The three-gluon Central-emission Vertex is evaluated at tree-level in the Regge limit. Higher order perturbative corrections to the theoretical predictions of Quantum Chromodynamics are required to match the experimental precision of particle colliders. The BFKL equation has previously been calculated up to next-to leading logarithmic order (NLL). Extending theoretical precision requires computing this equation to next-to-NLL (NNLL). A necessary ingredient for this is the three-gluon Central-emission Vertex.

Supervisors: Einar Gardi, Samuel Abreu

Personal statement

The first semester was a very steep learning curve. This was my first engagement with Quantum Field Theory so the background material was very difficult to engage with. I began by learning the basics of the spinor-helicity formalism and calculated some 6-pt amplitudes using the BCFW recursion relation. Then I moved on to reproducing results for the two-gluon CEV. I had some issues with this, not helped by the fact that I was new to Mathematica but eventually managed to reproduce the results over the Christmas break. At this point I wrote up a mini-report for semester 1.

In the second semester I began working on the three-gluon CEV. Progress was incredibly fast (since I had run into every possible problem last semester) and I was able to produce the first helicity configuration in the first few weeks. I then optimised my code and was able to produce the next two without issue. The final configuration was incredibly difficult and time-consuming. It required a lot of manual intervention in the code. Once I had all the configurations I began to develop the MRK, NMRK and soft checks and completed these just in time to put them in the report.

Before starting the project, I had very little idea of what Theoretical Physics research looked like. It has been a fantastic opportunity to dive into this world and I have greatly enjoyed being a part of research meetings.

Acknowledgments

I'd like to thank Yuyu Mo for his continued, enthusiastic engagement with my project. It was a pleasure to work with him.

Contents

1	Introduction	1
2	Helicity amplitudes in general kinematics	3
2.1	Yang-Mills / QCD	3
2.2	Spinor-helicity formalism	5
2.3	Properties of tree-level amplitudes	7
2.3.1	Conjugation	7
2.3.2	Colour decomposition	8
2.3.3	Soft Limits	8
2.4	MHV and NMHV amplitudes	9
2.5	BCFW recursion relation - building higher point amplitudes	9
2.5.1	BCFW example: (+ + + - -)	10
2.6	Helicity configurations	11
2.6.1	Colour-orderings	11
2.7	Obtaining CEV helicity configurations from amplitudes	12
2.7.1	A(- - - + + +)	13
2.7.2	B(- - + - + +)	13
2.7.3	C(- - + + - + +)	13
2.7.4	D(- + - + - + +)	14
3	The high-energy limit	15
3.1	Kinematics	15
3.2	Collider scenario	16
3.3	Regge kinematics	18
3.4	The Central-emission Vertex	20
3.5	Minimal set	21
4	Determining the three-gluon Central-emission Vertex	22
4.1	$A^{ggg(0)}(p_4^+; p_5^+, p_6^+)$	22
4.2	$A^{ggg(0)}(p_4^-; p_5^+, p_6^+)$	23
4.3	$A^{ggg(0)}(p_4^+; p_5^-, p_6^+)$	24
4.4	$A^{ggg(0)}(p_4^+; p_5^+, p_6^-)$	26
5	Analysis	28
5.1	Numerical check	28
5.2	NMRK and MRK limits	28
5.2.1	$A^{ggg(0)}(p_4^+; p_5^+, p_6^+)$ check	29
5.2.2	$A^{ggg(0)}(p_4^-; p_5^+, p_6^+)$ check	30
5.2.3	$A^{ggg(0)}(p_4^+; p_5^-, p_6^+)$ check	30
5.2.4	$A^{ggg(0)}(p_4^+; p_5^+, p_6^-)$ check	31
5.3	Soft check	32
5.3.1	Extraction of the two-gluon, same helicity CEV	32
5.3.2	Extraction of the two-gluon, opposite helicity CEV	33

6	Discussion	33
7	Conclusion	35
	Appendices	36
A	Obtaining the two-gluon CEV	36
B	Useful expressions in minimal variables	37

1 Introduction

The quest for knowledge and understanding has been a key element of human history. The development of the scientific method has allowed the quantification and understanding of a diverse range of phenomena, ranging from the scale of the universe to a fraction of the size of an atom. An interplay of theoretical prediction and experimental confirmation allows science to evolve. As technology advances, it is possible to investigate new limits; higher energy, smaller or larger distances. This inevitably reveals new behaviour and influences theory. Predictions (sometimes made a hundred years before being experimentally verified) are tested, and the theories which survive form our current understanding of the universe. Often, successful theories which are eventually disproved are correct as a limiting case of a more general theory. Newtonian gravity is fundamentally incorrect and was replaced by Einstein's Theory of General Relativity. However, it is still an accurate description in the limiting case of a 'weak' gravitational field and can predict with astonishing accuracy the orbits of almost all of the planets. If a theory has been tested repeatedly and no deviation from prediction has been found, there are two options. Either the theory is correct, or a limit where it breaks has not yet been probed. The general approach of physicists is to assume the second case.

This report evaluates the three-gluon Central-emission Vertex (CEV) at tree-level, an object which is extracted from the high-energy limit of a pure-gluon scattering amplitude. A scattering amplitude is the probability of a specified final state being produced from an initial state [1]. In particle physics, this is calculated using the machinery of Quantum Field Theory (QFT). Quantities which can be measured experimentally are referred to as observables. A scattering amplitude is not an observable but can be related to an observable cross-section. The evaluation of the three-gluon CEV is the first stage of a series of detailed calculations which construct a high-precision correction to the current theoretical predictions made by the Standard Model.

The Standard Model is a Quantum Field Theory (QFT) and is frequently referred to as the most accurate theory in physics. High-precision theoretical predictions of observable quantities can be calculated using a perturbative expansion, which is an infinite power series in a small expansion parameter. The contributions from these series become increasingly negligible as higher orders are considered. Yet since the series is infinitely long, predictions can always become more precise. Experimental results for scattering processes at particle colliders are currently more precise than theoretical calculations. This has generated an effort to calculate higher order corrections in perturbation theory to match the precision of the experimental results and test the accuracy of Standard Model at high energies [2].

The Large Hadron Collider (LHC) is the most advanced equipment in existence for studying subatomic particles [3]. Two beams of highly-relativistic protons are collided at sufficiently high energies that the protons can exchange gluons, which are usually confined to within hadrons [4, 5]. This causes the production of 'showers' of high-energy hadrons, called 'jets'. Cross-sections of these jets can be measured experimentally.

There are an enormous range of processes that can happen at colliders involving the strong,

weak and electromagnetic forces. The dominant processes involve the strong force [6] which is described using Quantum Chromodynamics (QCD). QCD is the study of interactions between quarks and gluons (which are collectively known as ‘partons’). These interact through the conserved charge of colour. Gluons are force-carrying bosons and are massless, meaning that they travel at the speed of light. They can be real or virtual. Real gluons are called ‘on-shell’ and virtual ones are ‘off-shell’.

QCD is a non-abelian theory which means that gluons ‘self-interact’; a gluon can produce another gluon. This implies the existence of ‘pure-gluon’ amplitudes, which do not contain quarks. Within the various QCD processes that take place in a particle collider, the leading contributions to the cross-sections of high-energy jets are given by pure-gluon emissions [7]. Of the contributions involving only gluons, ‘tree-level’ processes are dominant. These are the processes at the lowest order in perturbation theory and importantly do not contain ‘loops’ which require complicated renormalisation techniques.

Henceforth let us only consider QCD processes. The theoretical evaluation of the cross-section of a jet is a complex process which can be calculated using the BFKL (Balitsky-Fadin-Kuraev-Lipatov) equation [8–10]. The kernel of the BFKL is a resummed series in a parameter of the form $(\alpha_s \ln(s/|t|))$, where $(s/|t|)$ denotes the energy scale and α_s is the strong coupling constant which is small. The energy scale of particle colliders is very large, so the product $(\alpha_s \ln(s/|t|))$ can be of order unity. The leading logarithmic (LL) contributions come from terms which include $(\alpha_s \ln(s/|t|))^n$, where n is summed to infinity. The next-to-leading logarithmic (NLL) contributions come from $\alpha_s(\alpha_s \ln(s/|t|))^n$ terms. These are suppressed compared to LL contributions due to an additional factor of the coupling constant. In the high-energy limit, all the contributions have been calculated at LL order [11–14] and NLL order [15–18]. In order to extend QCD predictions to match experimental precision, contributions to the BFKL kernel at next-to NLL (NNLL) must now be included.

The pure-gluon ingredients needed for NLL and NNLL are represented in Figures 1 and 2. Note that NNLL contributions can be viewed either as taking NLL contributions to a higher loop degree or as having the emission of an additional gluon. The quantities in Figures 1 and 2 are represented as CEVs. An explanation of the CEV will be given in Section 3.4, after the relevant background has been covered. For now they should be thought of as useful objects that serve as building blocks.

In 2022, the 3-loop Regge trajectory [19] and the one-loop two-gluon CEV [20] were evaluated. There is current research ongoing in the Higgs Centre for Theoretical Physics (The University of Edinburgh) to calculate the two-loop one-gluon CEV. This leaves the tree-level three-gluon CEV as the final ingredient needed to compute the NNLL correction to the BFKL equation. An evaluation of the BFKL equation involves ‘interfering’ combinations of these CEVs with themselves or each other. The difficulty and importance of this task should not be underestimated, but our focus here will be solely on generating the three-gluon CEV.

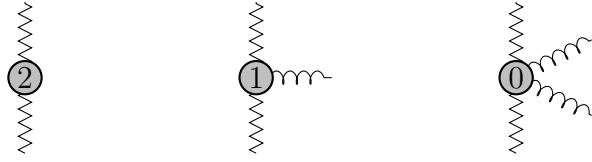


Figure 1. The diagrams contributing to the NLL approximation of the BFKL kernel. A circle represents a vertex, with the number corresponding to the number of loops. Zero represents tree-level (no loops). From left to right: 2-loop Regge trajectory, 1-loop single-gluon CEV, tree-level two-gluon CEV. Zig-zag lines represent Reggised gluons which will be discussed in Section 3.



Figure 2. The additional diagrams contributing to the NNLL approximation of the BFKL kernel. Right: tree-level three-gluon CEV, the focus of this report. NLL diagrams are also required at NNLL order.

Report structure

In Section 2 an overview of the ‘standard’ QFT approach to calculating scattering amplitudes is presented. It will become clear that a more systematic and efficient approach is required which will lead us to consider helicity. The spinor-helicity formalism is derived from Quantum Field Theory and methods for the classification and evaluation of helicity amplitudes are presented. In Section 3, the high-energy limit is discussed. This limit can be used to significantly simplify the difficult process of evaluating amplitudes. Even further simplification is available through the careful definition of a new set of dimensionless variables. A full definition of the Central-emission Vertex is then provided.

The results for the different helicity configurations which contribute to the three-gluon Central-emission Vertex at tree-level are presented in Section 4. These are analysed in Section 5 and it is shown that each result passes multiple tests. An outlook considering the uses for these results and steps for future research is given in Section 6.

2 Helicity amplitudes in general kinematics

2.1 Yang-Mills / QCD

Pure Yang-Mills theory is a non-abelian gauge theory that can be used to describe QCD without the presence of matter or fermions [21]. In most processes this is not a sufficient description since even pure-gluon amplitudes (where the initial and final states are all gluons)

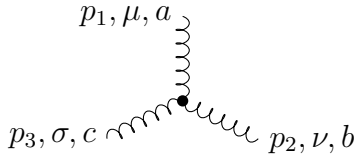
contain virtual quark-antiquark pair production and annihilation. However, within a pure-gluon scattering process any quark pairs would constitute a ‘loop’ which is higher order in the perturbative expansion. Any pure-gluon amplitude containing quarks would not be tree-level, so pure Yang-Mills theory is a sufficient description of QCD for our purposes. Henceforth we shall adopt the convention $c = \hbar = 1$ for convenience. The Yang-Mills Lagrangian is given by:

$$\mathcal{L} = -\frac{1}{4}F_{\mu\nu}^a F^{a\mu\nu} \quad (1)$$

with

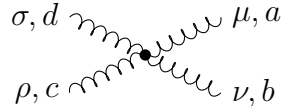
$$F_{\mu\nu}^a = \partial_\mu A_\nu^a(x) - \partial_\nu A_\mu^a(x) - ig[A_\mu^a(x), A_\nu^a(x)]. \quad (2)$$

The vector gauge field A_μ^a corresponds to a gluon with colour index a . Equation 1 is quadratic in $F_{\mu\nu}^a$ so the Lagrangian contains terms which are cubic and quartic in A_μ , due to the last term in Equation 2. This term is zero if the theory is abelian since the group elements would commute and its presence is directly responsible for the self-interaction of gluons. The cubic term, expressed as a Feynman vertex, is [6]



$$= g(if^{abc})i[\eta^{\mu\nu}(p_1^\sigma - p_2^\sigma) + \eta^{\nu\sigma}(p_2^\mu - p_3^\mu) + \eta^{\sigma\mu}(p_3^\nu - p_1^\nu)]. \quad (3)$$

The momentum p_i are taken as outgoing, $\{a, b, c\}$ are colour indices and $\eta_{\mu\nu} = \text{diag}(1, -1, -1, -1)$. The quartic term is



$$= ig^2[(if^{abe})(if^{ecd})(\eta^{\mu\rho}\eta^{\nu\sigma} - \eta^{\nu\rho}\eta^{\mu\sigma}) \\ + (if^{bce})(if^{ead})(\eta^{\nu\mu}\eta^{\rho\sigma} - \eta^{\rho\mu}\eta^{\nu\sigma}) \\ + (if^{cae})(if^{ebd})(\eta^{\rho\nu}\eta^{\mu\sigma} - \eta^{\mu\nu}\eta^{\rho\sigma})]. \quad (4)$$

We wish to extract the three-gluon CEV from the 7-pt amplitude $A_{\text{tree}}(gg \rightarrow ggggg)$. This must be computed first.

Given the task of computing the amplitude it is natural to first try the ‘standard’ procedure. This is to write down a Feynman diagram for every tree-level process with two initial and five final gluon states, then sum the contributions from each diagram using the Feynman rules. In principle every result presented in this report can be calculated in this manner, either by hand or computationally. The problem is that for a 7-pt tree-level gluon amplitude, there are 2,485 separate diagrams. If greater precision was ever desired (i.e NNNLL in the BFKL equation), an 8-pt tree-level amplitude would be needed in order to extract the four-gluon CEV. There are 34,300 separate diagrams for this amplitude. By the time a 10-pt amplitude is considered there are over 10 million diagrams [6].

Additionally, this is highly inefficient since many of the contributions from the diagrams will be power-suppressed when considering the typical energy scales of a particle collider. This will be discussed in greater detail in Section 3. A more systematic approach is needed, which is provided by considering the quantum spin of partons in the form of helicity.

2.2 Spinor-helicity formalism

Helicity is defined as the projection of a particle's spin onto its momentum vector [22]:

$$h = \frac{\vec{\mathbf{p}} \cdot \vec{\Sigma}}{2|\vec{\mathbf{p}}|} \quad , \quad \vec{\Sigma} \equiv \begin{pmatrix} \vec{\sigma} & 0 \\ 0 & \vec{\sigma} \end{pmatrix} \quad (5)$$

where $\vec{\sigma}$ is the Pauli vector. Helicity is not a conserved quantity for vector bosons such as the gluon (or the photon in Quantum Electrodynamics), but it is conserved for massless fermion interactions. Although massless fermions do not exist, at relativistic velocities fermion masses can be ignored as they are small compared to their kinetic energy. This makes a helicity a useful basis to consider, since there will be no contributions from fermion processes which violate helicity at high energies. As we will see in Section 2.4, expressing pure-gluon amplitudes in terms of helicity also orders the complexity of the amplitudes based on the degree of helicity 'violation'. This is already a great improvement in the pursuit of a systematic approach.

A brief derivation of the spinor-helicity formalism will now be covered. The interested reader can find more information here: [2, 6, 22, 23].

Let $\Psi(x)$ be a Dirac field whose equation of motion is given by the Dirac Equation,

$$(i\not{\partial} - m)\Psi(x) = 0. \quad (6)$$

By multiplying both sides by $(-i\not{\partial} - m)$ we generate the Klein-Gordon Equation.

$$(\partial^2 + m^2)\Psi(x) = 0. \quad (7)$$

This has solutions of the form

$$\Psi(x) = u(p)e^{ip \cdot x} + v(p)e^{-ip \cdot x}, \quad (8)$$

where $u(p)$ and $v(p)$ are Dirac spinors. This implies that

$$(i(\not{p}) - m)u(p)e^{ip \cdot x} + (i(-\not{p}) - m)v(p)e^{-ip \cdot x} = 0. \quad (9)$$

We have made no assumptions about the initial spinors $u(p)$ and $v(p)$. Therefore for the equation to be solved generally we must have

$$(\not{p} + m)u(p) = 0, \quad (10)$$

$$(-\not{p} + m)v(p) = 0. \quad (11)$$

This is an important result which reveals that in the absence of mass, the spinors $u(p)$ and $v(p)$ are solutions to the same equation: $\not{p}u = \not{p}v = 0$.

Let us write the Dirac spinor $u(p)$ in terms of Weyl spinors,

$$u(p) = \begin{pmatrix} \xi_- \\ \xi_+ \end{pmatrix}. \quad (12)$$

We can define

$$u_{\pm} = \frac{1}{2}(1 \pm \gamma^5) \quad \bar{u}_{\pm} = \frac{1}{2}\bar{u}(1 \mp \gamma^5), \quad (13)$$

so that $u = u_+ + u_-$. γ^μ are the gamma matrices in the chiral representation,

$$\gamma^\mu = \begin{pmatrix} 0 & \sigma^\mu \\ \bar{\sigma}^\mu & 0 \end{pmatrix}, \quad \gamma^5 = \begin{pmatrix} -1 & 0 \\ 0 & 1 \end{pmatrix} \quad (14)$$

and $\sigma^\mu \equiv (1, \sigma^i)$. Let us now assume that the fermions are highly relativistic and therefore have negligible mass, $m \approx 0$. Expanding Equation 10 we find

$$p_\mu \begin{pmatrix} 0 & \sigma^\mu \\ \bar{\sigma}^\mu & 0 \end{pmatrix} \begin{pmatrix} \xi_- \\ \xi_+ \end{pmatrix} = \begin{pmatrix} p_\mu \cdot \sigma \xi_+ \\ p_\mu \cdot \bar{\sigma} \xi_- \end{pmatrix} = 0 \quad (15)$$

This produces two equations, let us focus on ξ_+ . By using the standard representation for the Pauli matrices we have

$$p_\mu \sigma^\mu \xi_+ = (p_0 1 - p_1 \sigma^1 - p_2 \sigma^2 - p_3 \sigma^3) \xi_+ = 0 \quad (16)$$

$$\Rightarrow \begin{pmatrix} p_0 - p_3 & -p_1 + ip_2 \\ -p_1 - ip_2 & p_0 + p_3 \end{pmatrix} \xi_+ = 0. \quad (17)$$

These matrix elements inspire a use of ‘light-cone components’ which will be discussed in Section 3. For now they should be thought of as a convenient notation:

$$\begin{aligned} p^\pm &= p^0 \pm p^3 \\ p_\perp &= p^1 + ip^2 \\ p_\perp^* &= p^1 - ip^2 \end{aligned} \quad (18)$$

Equation 15 provides us with simultaneous equations which can be solved for ξ_+ . A similar matrix can be defined for ξ_- . The results are [22]

$$\xi_+ = \frac{1}{\sqrt{p^+}} \begin{pmatrix} p^+ \\ p_\perp \end{pmatrix}, \quad \xi_- = \frac{1}{\sqrt{p^+}} \begin{pmatrix} -p_\perp^* \\ p^+ \end{pmatrix}. \quad (19)$$

Since the massless forms of Equations 10 and 11 coincide, solutions of definite helicity can be chosen such that $u_\pm = v_\mp$ [23].

We define the ‘right-handed’ spinor product of gluons with momenta p and k consistent with Byrne *et al* [20],

$$\langle kp \rangle \equiv \langle k^- | p^+ \rangle = \bar{u}_-(k) u_+(p) = \xi_-^\dagger(k) \xi_+(p) = k_\perp \sqrt{\frac{p^+}{k^+}} - p_\perp \sqrt{\frac{k^+}{p^+}} \quad (20)$$

$$[kp] \equiv \langle k^+ | p^- \rangle = \xi_+^\dagger(k) \xi_-(p) = -k_\perp^* \sqrt{\frac{p^+}{k^+}} + p_\perp^* \sqrt{\frac{k^+}{p^+}} \quad (21)$$

The right and left handed products are related by complex conjugation.

$$[pk] = \text{sign}(k^0 p^0) \langle kp \rangle^* \quad (22)$$

To make use of momentum conservation, parton momenta must be defined consistently such that $\sum_{i=1}^n p_i^\mu = 0$. The convention here is that all momenta are taken as outgoing. Thus incoming partons are represented with negative energy and momenta, with their helicity value flipped. This produces an additional sign in the spinor products if the two partons are from different kinematic regions (i.e incoming/outgoing).

The products are anti-symmetric, as can be seen from Equations 20 and 21:

$$\langle pp \rangle = [pp] = 0 \quad , \quad \langle pk \rangle = -\langle kp \rangle \quad , \quad [pk] = -[kp],$$

and the scalar product of two four-momenta is defined as

$$p \cdot k = \frac{1}{2} \langle pk \rangle [kp]. \quad (23)$$

Note that

$$\langle k^- | k^- \rangle = \langle k^+ | k^+ \rangle = 0. \quad (24)$$

A projection operator can be defined

$$\not{p} = |p^+\rangle \langle p^+| + |p^-\rangle \langle p^-|, \quad (25)$$

and shorthand notation is introduced,

$$\langle a^+ | (\not{b} + \not{c}) | d^+ \rangle = \langle a^+ | b^- \rangle \langle b^- | d^+ \rangle + \langle a^+ | c^- \rangle \langle c^- | d^+ \rangle \equiv [a|(b+c)|d] \quad (26)$$

$$\langle a^- | (\not{b} + \not{c}) | d^- \rangle = \langle a^- | b^+ \rangle \langle b^+ | d^- \rangle + \langle a^- | c^+ \rangle \langle c^+ | d^- \rangle \equiv \langle a|(b+c)|d] \quad (27)$$

$$\langle a^- | (\not{b} + \not{c})(\not{d} + \not{e}) | f^+ \rangle \equiv \langle a|(b+c)(d+e)|f\rangle. \quad (28)$$

2.3 Properties of tree-level amplitudes

2.3.1 Conjugation

The helicity states of an amplitude can be reversed by complex conjugation,

$$[M(p_1^\nu, p_2^\nu, p_3^\nu, p_4^\nu, p_5^\nu, p_6^\nu, p_7^\nu)]^* = M(p_1^{-\nu}, p_2^{-\nu}, p_3^{-\nu}, p_4^{-\nu}, p_5^{-\nu}, p_6^{-\nu}, p_7^{-\nu}) \quad (29)$$

where ν labels the helicity state. In the previous section, spinor-helicity formalism was developed. It was stated that in the absence of mass there was degeneracy in the choice of representations between spinors $u(p), v(p)$. This choice should not affect any experimental measurement, which is consistent with the above equation since any measurement involves the absolute magnitude of an amplitude.

2.3.2 Colour decomposition

So far, discussion of colour has been limited. This is because at tree-level, it is possible to decompose amplitudes into the product of a trace involving colour and a ‘colour-stripped’ amplitude which only depends on helicity and momentum,

$$M_n^{tree}(1, 2, \dots, n) = g^{n-2} \sum_{\sigma \in S_n / \mathbb{Z}} \text{Tr}(T^{a_{\sigma_1}} \dots T^{a_{\sigma_n}}) A_n^{tree}(\sigma(1_1^\nu) \dots \sigma(n_1^\nu)). \quad (30)$$

g is related to the QCD coupling constant. The sum is over the cyclic permutations which generate new independent traces [22].

This means that at tree-level, colour does not play an important role in our analysis. Henceforth only colour-stripped amplitudes will be considered and will frequently just be referred to as ‘amplitudes’.

2.3.3 Soft Limits

If a gluon is emitted with very low momenta ($p_i \approx 0$) the amplitude becomes singular due to a division by zero. This is called a ‘soft’ emission. In Quantum Field Theory, singularities occur when the propagator corresponding to a particle goes on-shell. Final state gluons must be on-shell. Consider a final state gluon with momentum p that was emitted from an off-shell gluon which also produced a soft gluon. Momentum conservation implies $p_{\text{off-shell}} = (p_{\text{soft}} + p) \approx p$. Therefore the soft gluon it is approximately on-shell, which is the physical source of this singularity.

In the soft-limit, the n -pt tree-level amplitude factorises into a singular factor multiplied by an $(n - 1)$ -pt amplitude with the soft gluon removed [22],

$$A_{tree}^n(1, \dots, p, s, q, \dots, n) = S(p, s^\pm, q) A_{tree}^{n-1}(1, \dots, p, q, \dots, n). \quad (31)$$

The singular $S(p, s^\pm, q)$ is known as the eikonal factor which depends on the helicity of the soft gluon,

$$S(p, s^+, q) = \frac{\langle pq \rangle}{\langle ps \rangle \langle sq \rangle}, \quad (32)$$

$$S(p, s^-, q) = -\frac{[pq]}{[ps][sq]}. \quad (33)$$

The eikonal factor is independent of spin; since a low-energy gluon has a long wavelength, it can be considered to be classical in comparison to the high-energy process which emitted it.

2.4 MHV and NMHV amplitudes

An n -pt tree level amplitude can be written as the sum of partial-amplitudes which are categorised by a helicity configuration such as $(p_1^+, p_2^+, p_3^+, p_4^-, p_5^-, p_6^-, p_7^-)$. Generally, partial-amplitudes are non-zero and are complicated to evaluate. However, many of these configurations contain a ‘helicity flip’ impact factor.

$$C^{g(0)}(p_2^\pm, p_3^\pm), \quad C^{g(0)}(p_1^\pm, p_7^\pm)$$

Note that due to the ‘all-outgoing’ momentum convention, the helicity of initial partons have been reversed. As we will see in Section 3, the partial-amplitudes which contain a helicity flip impact factor are power-suppressed and approach zero in the high-energy limit.

At tree-level, non-helicity-violating impact factors are represented by a phase factor. It is convenient to set one of these to be 1 [20].

$$C^{g(0)}(p_2^-, p_3^+) = 1, \quad C^{g(0)}(p_1^-, p_7^+) = \frac{q_{3\perp}^*}{q_{3\perp}}. \quad (34)$$

If every parton has the same helicity or only one parton has different helicity, the amplitude is zero. Partial amplitudes are ordered in complexity based on their degree of helicity violation. The simplest non-zero amplitudes are called Maximally Helicity Violating (MHV). In an MHV amplitude, all but two gluons are of the same helicity.

All MHV amplitudes can be obtained through the expression [24].

$$A_{jl}^{\text{MHV}} \equiv A_n^{\text{tree}}(1^+, \dots, j^-, \dots, l^-, \dots, n^+) = \frac{\langle jl \rangle^4}{\langle 12 \rangle \dots \langle n1 \rangle}. \quad (35)$$

MHV amplitudes that have all but two negative helicity gluons are obtained by conjugation and use of the anti-symmetric property of spinor-products.

$$A_{jl}^{\text{MHV}} \equiv A_n^{\text{tree}}(1^-, \dots, j^+, \dots, l^+, \dots, n^-) = (-1)^n \frac{[jl]^4}{[12] \dots [n1]} \quad (36)$$

Amplitudes with all but three positive or all but three negative helicity gluons are called Next-to-Maximally-Helicity violating (NMHV) amplitudes. For $n < 8$ only MHV and NMHV amplitudes exist.

2.5 BCFW recursion relation - building higher point amplitudes

Britto et al. [25] present a recursion relation for colour-stripped amplitudes which allows higher point tree-level amplitudes to be built from lower ones. Amplitudes are decomposed into a sum of products of lower point amplitudes, connected by an on-shell propagator.

$$iA_n(p_1, \dots, p_n) = \sum_{h=\pm} \sum_{k=2}^{n-2} \left[iA_{k+1}(\hat{1}, 2, \dots, k, -\hat{P}_{1,k}^{-h}) \frac{i}{P_{1,k}^2} iA_{n-k+1}(\hat{P}_{1,k}^h, k+1, \dots, \hat{n}) \right], \quad (37)$$

where n is the number of on-shell gluons. As usual, a singularity arises in the case that the propagator $P^2 = 0$. The amplitude can be evaluated by analytic continuation. Momenta are complexified and ‘shifted’ in such a way that preserves both momentum conservation and the on-shell condition $p^2 = 0$.

The following notation is defined,

$$\begin{aligned} \{\lambda_a(p) = \xi_+(p), \quad \lambda^a(p) = \xi_-^\dagger(p)\} \\ \{\tilde{\lambda}^{\dot{a}}(p) = \xi_-(p), \quad \tilde{\lambda}_{\dot{a}}(p) = \xi_+^\dagger(p)\}. \end{aligned}$$

This momentum shift is equivalent to a shift on the spinors $\lambda_a(p)$, $\tilde{\lambda}_{\dot{a}}(p)$ via shift vectors r_i^μ . A simple shift known as the $|6^-, 1^+\rangle$ shift [23] is to have $r_i^\mu = 0$ for $i \in \{2, 3, 4, 5\}$ and

$$\begin{cases} \hat{\lambda}_1 = \lambda_1 + z\lambda_6 & \hat{\tilde{\lambda}}_1 = \tilde{\lambda}_1 \\ \hat{\lambda}_6 = \lambda_6 & \hat{\tilde{\lambda}}_6 = \tilde{\lambda}_6 - z\tilde{\lambda}_1. \end{cases}$$

In terms of spinor products this translates to

$$\begin{cases} |\hat{1}^-\rangle = |1^-\rangle & |\hat{6}^+\rangle = |6^+\rangle \\ |\hat{1}^+\rangle = |1^+\rangle + z|6^+\rangle & |\hat{6}^-\rangle = |6^-\rangle - z|1^-\rangle. \end{cases} \quad (38)$$

The location of the pole is [22]

$$z = -\frac{P_{1,k}^2}{\langle n^- | P_{1,k} | 1^+ \rangle} \quad , \quad P_{1,k} \equiv \left(\sum_{i=1}^k p_i \right)^2. \quad (39)$$

The earlier work of Parke and Taylor [24] provided a very simple equation for evaluating MHV amplitudes (Equation (35)). The BCFW relation can build all higher point amplitudes from $n \geq 3$ and $n = 3$ gluon amplitudes contain only MHV amplitudes. Therefore, all tree-level amplitudes can be calculated from Parke and Taylor’s MHV formula.

2.5.1 BCFW example: (+ + + - - -)

The $k = 2$ portion of Equation (37) for $n = 6$ is presented as an example.

$$iI_2 = \sum_{h=\pm} iA_3 \left(\hat{1}^+, 2^+, -\hat{P}_{1,2}^{-h} \right) \frac{i}{P_{1,2}^2} A_5 \left(\hat{P}_{1,2}^{+h}, 3^+, 4^-, 5^-, \hat{6}^- \right). \quad (40)$$

Due to helicity conservation, only ($h = +$) terms survive since otherwise A_3 is zero. The remaining task is to evaluate A_3 and A_5 – which are both MHV amplitudes, and recover the result for un-shifted momenta.

$$\begin{aligned}
iA_3 \left(\hat{1}^+, 2^+, -\hat{P}_{1,2}^- \right) &= -i \frac{[12]^4}{[12][2(-\hat{P}_{1,2}^-)][(-\hat{P}_{1,2}^-)1]} \\
&= i \frac{[12]^3}{[2\hat{P}_{1,2}][\hat{P}_{1,2}1]},
\end{aligned}$$

where we have noted that $[k(-\hat{P}_{1,2})] = i[k\hat{P}_{1,2}]$. Similarly we have

$$\begin{aligned}
iA_5 \left(\hat{P}_{1,2}^+, 3^+, 4^-, 5^-, \hat{6}^- \right) &= -\frac{[\hat{P}_{1,2}^+ 3]^4}{[\hat{P}_{1,2}^+ 3][34][45][45][5\hat{6}][\hat{6}\hat{P}_{1,2}^+]} \\
&= -\frac{[\hat{P}_{1,2}^+ 3]^3}{[34][45][45][5\hat{6}][\hat{6}\hat{P}_{1,2}^+]}.
\end{aligned}$$

Using Equation (39) we find $z = -\frac{\langle 12 \rangle}{\langle 62 \rangle}$.

Multiplying the expression by $\frac{\langle 6\hat{P} \rangle^3}{\langle 6\hat{P} \rangle^3}$ and simplifying, we reach the final answer:

$$iI_2 = \frac{i}{s_{126}} \frac{\langle 6^- | p_1 + p_2 | 3^- \rangle^3}{\langle 12 \rangle \langle 61 \rangle [34][45] \langle 2^- | p_1 + p_6 | 5^- \rangle}. \quad (41)$$

In the shorthand notation introduced in Section 2.2, this is

$$iI_2 = \frac{i}{s_{126}} \frac{\langle 6|(1+2)|3 \rangle^3}{\langle 12 \rangle \langle 61 \rangle [34][45] \langle 2|(1+6)|5 \rangle}. \quad (42)$$

2.6 Helicity configurations

2.6.1 Colour-orderings

It is very important to note that before any kinematic limits have been taken, the expression for a helicity amplitude (for example an MHV or NMHV) is completely general. This allows complete freedom in relabelling what we refer to as the first gluon, second gluon and so on. In certain situations, as we will see in Section 4, this can allow a helicity configuration of the CEV to be generated from an amplitude that would otherwise be suppressed in the high-energy limit. This labelling is called a ‘colour-ordering’ and the standard order is ‘A-type’ which is $(1, 2, 3, \dots, n)$. The relation to colour is the ordering of the generators in the trace which accompanies the colour-stripped amplitude to give the full expression. A consistent relabelling of partons must also relabel the generators in the trace.

Any configuration of partons can be used, but not all are useful. In the results presented in Section 4, a ‘B-type’ colour ordering is used. This is obtained by ‘swapping’ the second and fourth partons in an A-type configuration: $(1, 4, 3, 2, 5, 6, 7)$. This specific ordering has gluon 4 in the ‘incoming’ kinematic region, hence it’s momentum value will gain a minus sign.

It is essential to note that by a ‘swap’ we mean a swap solely of the parton’s momentum p_i . An equation for a helicity amplitude is defined by the adjacency of positive and negative helicity gluons. If the helicity were also swapped with the momentum the equation would no longer be correct, it would be a completely different amplitude. A useful property of traces is that they are invariant under cyclic permutations:

$$\text{tr}(ABCD...) = \text{tr}(BCD...A) = \text{tr}(CD...AB) = \dots \quad (43)$$

This means that $(4, 3, 2, 5, 6, 7, 1), (3, 2, 5, 6, 7, 1, 4), \dots$, will all generate a B-type CEV.

2.7 Obtaining CEV helicity configurations from amplitudes

In general, an amplitude can be difficult and time consuming to evaluate. It would be efficient to be able to extract multiple CEV configurations from each amplitude. A 3-CEV has a total of $2 \times 2 \times 2 = 8$ helicity configurations. Four of these are independent as the remaining four can be generated by conjugation (swapping positive and negative helicity states).

As discussed in Section 2.4, amplitudes which contain a helicity-flip factor are power suppressed in $|t|/s$. The CEV cannot be extracted from a suppressed amplitude so these are not of interest. This means that we will only consider amplitudes where gluons 1 and 7 have opposite helicities as well as gluons 2 and 3.

There is no simple relation between different colour orderings and therefore all CEV configurations should be generated in one colour ordering, which in this case is B-type. A systematic approach is needed to discover which CEV configurations can be obtained from an amplitude. The conditions are summarised below:

- The helicity configuration of an amplitude must remain the same
- Gluons can be relabelled giving a different colour-ordering, but the same ordering should be used for all configurations
- By exploiting the cyclic property of the trace, the labelling of gluons can be cycled without changing the type of colour-ordering.
- A CEV cannot be generated from a power suppressed amplitude.

A systematic approach, consistent with these conditions, is explained in analogy to the combination lock of a safe. The inner ring is the helicity configuration and this is fixed for a given amplitude. The outer ring represents the labelling of the gluons and must have the correct order, but can rotate around the inner ring. There are four independent partial-amplitudes associated with the 7-pt amplitude which are presented in Bern et al. [26]. From these, all other amplitudes can be generated via manipulations such as reflection and conjugation.

The following amplitudes correspond to amplitudes A-D in Bern *et al*’s paper. All of the non-suppressed three-gluon CEV configurations are extracted using the notation $(\nu_4; \nu_5, \nu_6)$. The

$(+; +, +)$ configuration can, for obvious reasons, only be generated from an MHV amplitude and so does not appear in the following analysis. This is the only configuration obtainable from an MHV amplitude. Explicit expressions for the amplitudes are provided in Section 4, for now the analysis will remain qualitative.

2.7.1 A(- - - + + + +)

$$= (-; +, +) \quad (44)$$

2.7.2 B(- - + - + + +)

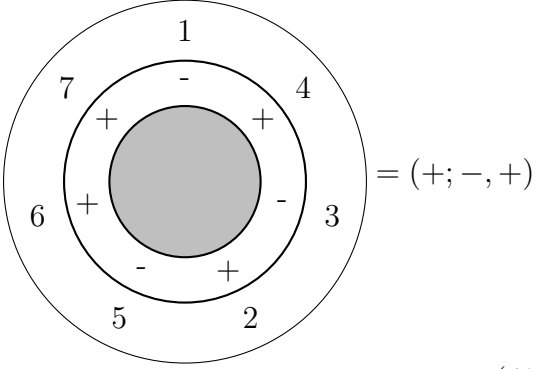
$$= (-; +, +) \quad (45)$$

$$= (+; -, +) \quad (46)$$

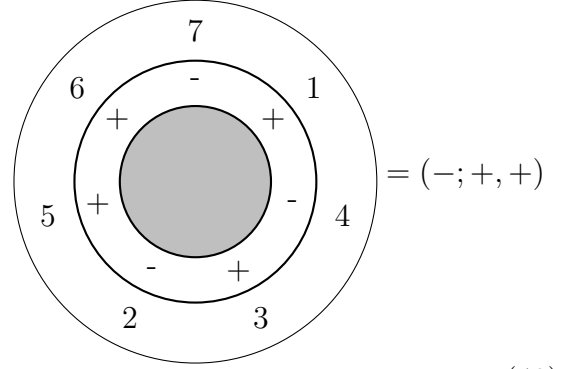
2.7.3 C(- - + + - + +)

$$= (+; -, +) \quad (47)$$

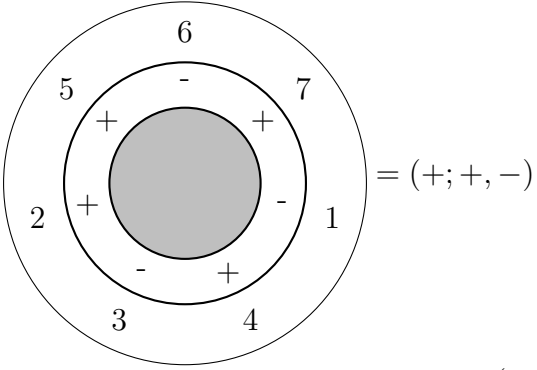
2.7.4 D(- + - + - + +)



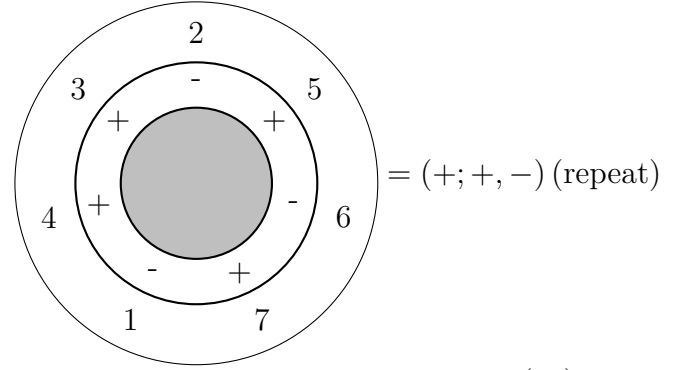
(48)



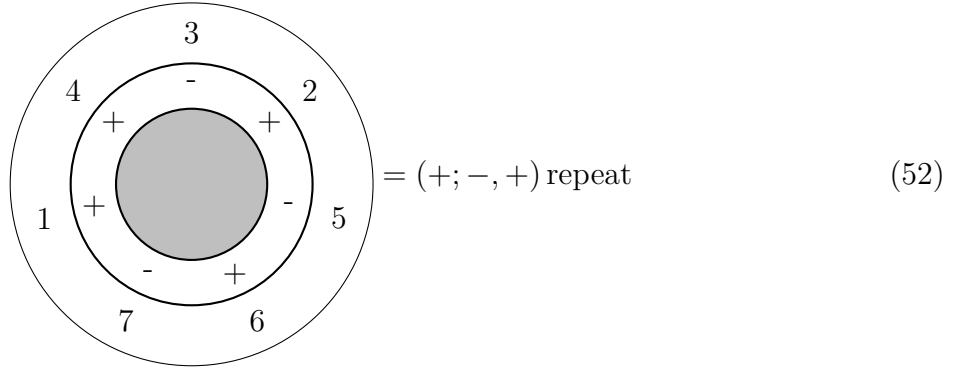
(49)



(50)



(51)



(52)

The last amplitude is the most fruitful in terms of configurations. It can generate all of the configurations apart from $(+; +, +)$. However it is also the most complicated to evaluate, owing to its lack of helicity symmetry. Amplitudes with higher symmetry were favoured over this in an attempt to minimise errors. For example the $(-; +, +)$ configuration can be generated from the A amplitude which contains only three terms rather than the six needed for D.

The B amplitude is unique in giving a new CEV configuration if the colour ordering is reversed, i.e $(7, 6, 5, 2, 3, 4, 1)$ rather than $(1, 4, 3, 2, 5, 6, 7)$. This is still a B-type configuration.

$$= (+; +, -) \quad (53)$$

Reversing the colour ordering in the other amplitudes either generates suppressed configurations or configurations that can already be obtained from that amplitude.

3 The high-energy limit

Having developed a systematic and efficient method for calculating pure-gluon amplitudes, we turn our focus to the limit in which initial gluons have very high momentum. This is useful because it simplifies the physics behind the interaction. It is also necessary to consider this limit since it is quintessential of particle colliders. We begin by returning to the light-cone components that were briefly introduced in Section 2.2.

3.1 Kinematics

We choose to make a variable transformation to light-cone components. Expressed in terms of cartesian components, this is

$$\begin{aligned} p^\pm &= p^0 \pm p^3 \\ p_\perp &= p^1 + ip^2 \\ p_\perp^* &= p^1 - ip^2. \end{aligned}$$

The p^\pm components are ‘longitudinal’ and $p_\perp^{(*)}$ are ‘perpendicular’. In the analysis of Section 2.2, the light-cone components appeared unexpectedly. This is because they are the natural choice of coordinates to express light-like vectors.

The scalar product is invariant,

$$\begin{aligned} 2p \cdot q &= p^+ q^- + p^- q^+ - p_\perp^* q_\perp - p_\perp q_\perp^* \\ \Rightarrow p \cdot p &= p^+ p^- - p_\perp p_\perp^*. \end{aligned} \quad \begin{aligned} (54) \\ (55) \end{aligned}$$

It should be noted that there is a notation clash where $(+, -)$ are used to represent light-cone coordinates and helicity, however the meaning is always obvious from context. For example, any signs appearing in an amplitude refer to helicity but $p_4^+ \rightarrow 0$ would refer to the plus momentum component of p_4 .

The on-shell condition for a light-like (massless) vector is $p_\mu p^\mu = 0$, which is invariant. This must be true in all frames, for all choices of coordinates and thus extends to light-cone components. From Equation 55, the on-shell condition is:

$$p^+ p^- = p_\perp p_\perp^* \quad (56)$$

All external states must be on-shell.

3.2 Collider scenario

In a hadron collider two beams of hadrons are accelerated towards each other so that the particles collide head-on. In the LHC, these are protons and travel up to 99.9999991% the speed of light [3]. At this highly relativistic velocity, a proton in one beam sees the approaching beam as being extremely time-dilated and thus interacts with it as if it was a stationary distribution of partons [10]. There will be quark-quark, quark-gluon and pure-gluon scattering but we will focus on the latter here.

Two initial on-shell gluons are taken to collide head-on along the z -axis,

$$\begin{aligned} p_1 &= (|p_1^z|, 0, 0, p_1^z) \\ p_2 &= (|p_2^z|, 0, 0, p_2^z). \end{aligned}$$

By requiring that particle 1 has z component momentum $\frac{-p_1^-}{2}$ and particle 2 has $\frac{p_2^+}{2}$, we can write [22]

$$\begin{aligned} p_1^{\text{LC}} &= -(0, p_1^-; 0, 0) \\ p_2^{\text{LC}} &= -(p_2^+, 0; 0, 0). \end{aligned} \quad (57)$$

in the notation $p^{\text{LC}} = (p^+, p^-; p_\perp, p_\perp^*)$. The minus signs arise from the outgoing momentum convention.

The momenta of p_1 and p_2 are very large. To see the effects of this we consider the simplest example of a pure-gluon process: $2 \rightarrow 2$ scattering. These are processes which have two initial and two final gluons, and we will only consider tree-level.

The Mandelstam variables are:

$$s = (p_1 + p_2)^2 = (p_3 + p_4)^2 \quad (58)$$

$$t = (p_1 - p_3)^2 = (p_4 - p_2)^2 \quad (59)$$

$$u = (p_1 - p_4)^2 = (p_3 - p_2)^2, \quad (60)$$

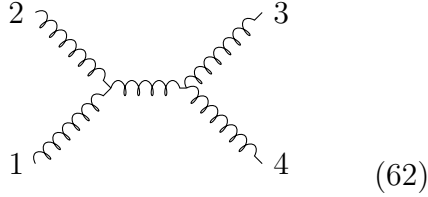
$$(61)$$

where s is called the centre of mass energy (squared) and t is the four-momentum transfer (squared). Intuition from the classical scattering of two massive objects is that particles colliding head on at high velocities keep most of their momentum. The objects continue moving

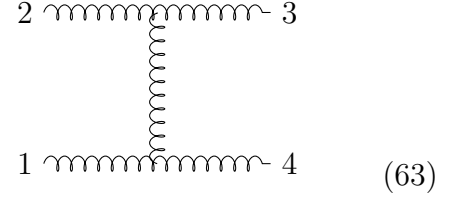
roughly in the same direction and the exchange of momentum between objects is much less than either of the object's initial momentum. In terms of the Mandelstam invariants, this corresponds to $s \gg |t|$.

This intuition extends to gluon scattering and is known as the ‘Regge limit’ [27], which will be discussed in the next section. In this limit, the probability that initial gluon 2 is the same parton as final state gluon 3 is very high (likewise for 1 and 4). Therefore amplitudes which contain a helicity-flip impact factor (as discussed in Section 2.4) are power-suppressed in t_3/s_{12} and/or t_1/s_{12} . In the high energy limit these partial-amplitudes approach zero. For massless particles, $s + t + u = 0$ so in the high-energy limit we have $s \approx -u$.

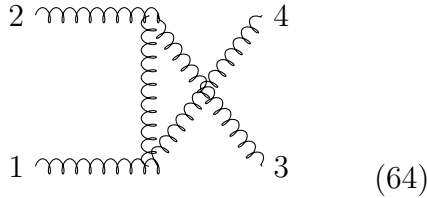
There are four Feynman diagrams associated with general $2 \rightarrow 2$ scattering which are shown in Figures 62 - 65.



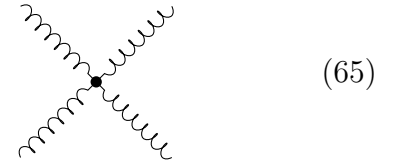
s-channel diagram



t-channel diagram



u-channel diagram



4-gluon vertex

The s -channel propagator is proportional to $1/s$ and the t -channel propagator to $1/t$ so the s -channel is suppressed in $|t|/s$. Similarly the u -channel is suppressed in $|t|/(u) \approx |t|/(-s)$. The 4-gluon vertex does not contain a propagator, and so in the limit $s \gg |t|$, the t -channel becomes dominant. The analysis here extends to higher point amplitudes and therefore we will only t -channel processes from now on.

A diagram for a 7-pt amplitude can now be constructed in momentum space (Figure 3). For simplicity, gluons have been represented with straight lines. Note the direction of the arrows, the initial particles are represented as having negative outgoing momentum. Initially

we make no assumptions about the momenta of central particles (4,5 and 6).

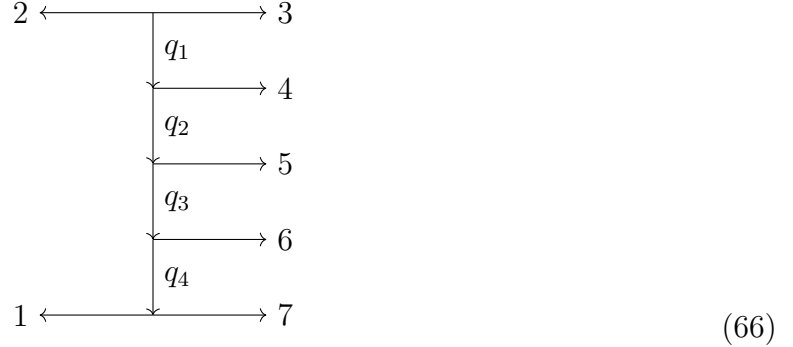


Figure 3. A diagram of the 7-pt pure-gluon tree-level amplitude.

3.3 Regge kinematics

In the previous section we introduced the Regge limit $s \gg |t|$ and proposed appropriate initial conditions for the momenta of the incoming gluons. In this section we investigate how this simplifies the physics.

The properties of the propagators q_1 and q_4 can be investigated in the Regge limit, based on the set-up of Equation 57. We begin by writing down the components for p_3 .

$$p_3 = (p_3^+, p_3^-, p_{3\perp}, p_{3\perp}^*) \quad (67)$$

As discussed above, we expect gluon 3 to have similar momentum to gluon 2. This means that $p_3^+ \gg p_3^-, p_{3\perp}$. Let us introduce a scaling parameter $\lambda \propto \mathcal{O}(|t|/s) \approx 0$. As gluon 3 is an external state, it must be on-shell so $p_3^2 = 0 = p_3^+ p_3^- - |p_{3\perp}|^2$. Therefore in terms of orders of magnitude we can write $p_3^+ \approx (-p_2^+)$, $p_3^- \approx \lambda(-p_2^+)$ resulting in $p_{3\perp} \approx \sqrt{\lambda}(-p_2^+)$.

$$p_3 \approx -p_2^+(1, \lambda, \sqrt{\lambda}, \sqrt{\lambda}) \quad (68)$$

By use of momentum conservation at the top vertex we can deduce

$$q_1 = -(p_2 + p_3) = p_2^+(0, \lambda, \sqrt{\lambda}, \sqrt{\lambda}). \quad (69)$$

By following a similar argument at the lowest vertex we find

$$q_4 = -(p_1 + p_7) \approx p_1^-(\lambda, 0, \sqrt{\lambda}, \sqrt{\lambda}). \quad (70)$$

Now q_1 and q_4 can be compared. No assumptions have been made about particles 4,5 and 6 and thus entirely in terms of orders of magnitude we can write: $q_1 \approx q_4$ by using momentum

conservation at each of the central vertices. Noting that p_1^- and p_2^+ are of the same order of magnitude, it is concluded that

$$q_1, q_4 \approx (0, 0, \sqrt{\lambda}, \sqrt{\lambda}). \quad (71)$$

Of course, the zero represents a small component compared to the other components and not exactly zero. The conclusion is that in the Regge limit only perpendicular momentum is exchanged in the t -channel. Under these conditions, the propagator is known as a ‘Reggiezed gluon’ [9].

The most general case of the Regge limit makes no assumptions about the momenta of central partons. For a 7-pt amplitude, this is called next-to-next-to-Multi-Regge Kinematics (NNMRK),

$$\begin{aligned} p_3^+ &\gg p_4^+ \approx p_5^+ \approx p_6^+ \gg p_7^+ \\ p_3^- &\ll p_4^- \approx p_5^- \approx p_6^- \ll p_7^-, \end{aligned} \quad (72)$$

with each particle having comparable transverse momenta

$$|p_{3\perp}| \approx |p_{4\perp}| \approx |p_{5\perp}| \approx |p_{6\perp}| \approx |p_{7\perp}|. \quad (73)$$

The next-to MRK (NMRK) limit is achieved by assuming that the longitudinal momentum of one of the central partons is much greater (or much less than) the other two, for example

$$\begin{aligned} p_3^+ &\gg p_4^+ \gg p_5^+ \approx p_6^+ \gg p_7^+ \\ p_3^- &\ll p_4^- \ll p_5^- \approx p_6^- \ll p_7^-. \end{aligned} \quad (74)$$

Finally, the strictest limit is the MRK limit which assumes a strong hierarchy between all partons,

$$\begin{aligned} p_3^+ &\gg p_4^+ \gg p_5^+ \gg p_6^+ \gg p_7^+ \\ p_3^- &\ll p_4^- \ll p_5^- \ll p_6^- \ll p_7^-. \end{aligned} \quad (75)$$

Based on the kinematic set up in Equation 57, the plus component of the momentum of the final five gluons will come entirely from initial gluon 2. Similarly, the negative components will come entirely from gluon 1. As there is a consistent definition of momenta (all outgoing), we can use momentum conservation,

$$-p_2^+ = \sum_{i=3}^7 p_i^+ \quad (76)$$

$$-p_1^- = \sum_{i=3}^7 p_i^-. \quad (77)$$

Following a similar reasoning, the initial gluons have no transverse momentum components and thus

$$\sum_{i=3}^7 p_{i\perp} = 0. \quad (78)$$

As we will see in Section 5, the MRK and NMRK limits lead to factorisation and simplification of the general NNM RK result.

3.4 The Central-emission Vertex

Finally, we have reached the point where a definition of the CEV can be given. In the Regge limit, a general colour-stripped amplitude factorises completely into the product of ‘central’ (exchanged in the t-channel) and non-central quantities.

$$M_{6g}^{(0)}(p_1^{\nu_1}, p_2^{\nu_2}, p_3^{\nu_3}, p_4^{\nu_4}, p_5^{\nu_5}, p_6^{\nu_6}, p_7^{\nu_7}) = s_{12} C^{g(0)}(p_2^{\nu_2}, p_3^{\nu_3}) \frac{1}{t_1} A^{ggg(0)}(q_{1\perp}, p_4^{\nu_4}, p_5^{\nu_5}, p_6^{\nu_6}, q_{4\perp}) \frac{1}{t_4} C^{g(0)}(p_1^{\nu_1}, p_6^{\nu_6}) \quad (79)$$

With ν representing either positive or negative helicity and the impact factors as defined in Section 2.4. The Mandelstam invariants are similar to the ones introduced for $2 \rightarrow 2$ scattering in Section 3.2. In the NNMRK limit of $2 \rightarrow 5$ scattering, $s = p_3^+ p_7^-$, $t_i \approx -|q_{i\perp}|^2$.

This allows an extraction of the Central-emission Vertex

$$A^{ggg(0)}(q_{1\perp}, p_4^{\nu_4}, p_5^{\nu_5}, p_6^{\nu_6}, q_{4\perp}) \quad (80)$$

This is represented diagrammatically in Figure 4 and 5. CEVs are categorised based on the number of on-shell gluons they emit. It is convenient to introduce the shorthand ‘ m -CEV’ to describe a CEV which emits m gluons.

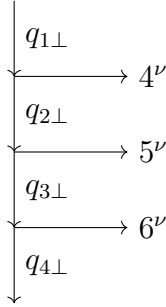


Figure 4. A schematic diagram of an A-type 3-CEV in momentum space.

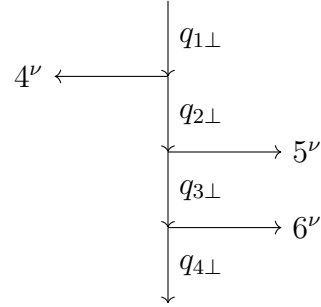


Figure 5. A schematic diagram of a B-type 3-CEV in momentum space.

We will see in Section 5 that in the NMRK and MRK limits, a CEV factorises into products of smaller CEVs connected by propagators. It can therefore be thought of as a ‘building block’ which will be discussed further in Section 5. In preparation for this and as common in QFT, the propagators corresponding to $q_{1\perp}$ and $q_{4\perp}$ have been amputated in the definition of the CEV.

The m -gluon CEV can be thought of as an off-shell amplitude, where two initial off-shell gluons of momenta $q_{1\perp}$ and $q_{4\perp}$ produce m final gluons.

We define the following useful quantities by using momentum conservation at each vertex in Figure 4,

$$q_{1\perp} = -p_{3\perp} - p_{2\perp} = -p_{3\perp} \quad (81)$$

$$q_{3\perp} = p_{6\perp} + p_{1\perp} = p_{6\perp} \quad (82)$$

$$q_{2\perp} = p_{5\perp} + q_{3\perp}. \quad (83)$$

$$(84)$$

An n -pt amplitude in 4-dimensional space-time has mass-dimension $n - 4$ [23]. In the units $c = \hbar = 1$, mass has the same dimension as momentum. Therefore the dimension of the CEV can be determined from Equation 79. The impact factors are dimensionless and s_{12} and t_i have dimensions of momentum squared. An $n = 7$ gluon amplitude has mass dimension $n - 4$ and therefore the 3-CEV has a dimension of inverse momentum. In general, the CEV of an n -pt amplitude has mass-dimension $6 - n$ which implies an m -CEV has dimension $2 - m$.

3.5 Minimal set

Light-cone components are the natural choice for expressing light-like particles such as gluons. However conditions such as momentum conservation at each vertex in the Feynman diagram and the on-shell condition $p_i^+ p_i^- = |p_{i\perp}|^2$ can allow us to eliminate degrees of freedom. For example, each p_i^+ can be replaced with $|p_{i\perp}|^2 / p_i^-$. The number of physical degrees of freedom in the scattering process is less than the number of variables and so it is expected that the results can be presented in a more compact form by using carefully constructed variables - the minimal set. This concept was first presented in Byrne et al. [20].

Consider a high-energy n -gluon tree-level CEV as in Figure 4. Considering only momentum (and not colour and helicity), each gluon carries three degrees of freedom due to the on-shell relation. Momentum conservation removes an overall degree of freedom and thus the number of degrees of freedom needed to express this system is:

$$N = 3n - 1 \quad (85)$$

Evaluating this expression $n = 3$ gives 8 degrees of freedom. There is a large degree of choice in a set of minimal variables. The variables chosen here are:

$$\{z_1, \bar{z}_1, z_2, \bar{z}_2, z_3, \bar{z}_3, X, Y\} \quad (86)$$

$$z_1 = \frac{q_{2\perp}}{p_{4\perp}}, \quad z_2 = \frac{q_{2\perp}}{p_{5\perp}}, \quad z_3 = \frac{q_{3\perp}}{p_{6\perp}}, \quad X = \frac{p_4^+}{p_5^+}, \quad Y = \frac{p_5^+}{p_6^+} \quad (87)$$

Note that the minimal set, which is used to express the CEV, only depends on ‘central quantities’.

An additional benefit of this choice of minimal variables is that they are dimensionless which means that dimensional analysis of results is particularly simple. The results in the following section are expressed in terms of minimal variables. Converting from light-cone coordinates to the minimal set is non-trivial. In preparation for this some useful quantities are derived in Appendix B.

4 Determining the three-gluon Central-emission Vertex

The results in this section were computed using code written in `Mathematica`. The files are available here [28]. The four independent helicity configurations contributing to the three-gluon CEV are evaluated in the NNMRK limit. The remaining four configurations correspond to swapping the positive and negative helicity states of these independent configurations and can be obtained through complex conjugation as shown in Equation 29. It is useful to compute the 2-CEV as it can be used to check the consistency of the 3-CEV results. This can be found in Appendix A.

A significant simplification is to take a different colour ordering. The following results are calculated in a B-type colour ordering obtained by swapping the momenta of particles 2 and 4 in the standard (A-type) ordering,

$$M_{7g}^{\text{A-type}}(p_1^{\nu_1}, p_2^{\nu_2}, p_3^{\nu_3}, p_4^{\nu_4}, p_5^{\nu_5}, p_6^{\nu_6}, p_7^{\nu_7}) \rightarrow M_{7g}^{\text{B-type}}(p_1^{\nu_1}, p_4^{\nu_2}, p_3^{\nu_3}, p_2^{\nu_4}, p_5^{\nu_5}, p_6^{\nu_6}, p_7^{\nu_7}).$$

Note that the helicities do not change with the ordering. A B-type CEV is written using the concise notation

$$A^{ggg(0)}(p_4^{\nu_4}; p_5^{\nu_5}, p_6^{\nu_6}) \equiv A_{\text{B-type}}^{ggg(0)}(q_1, p_4^{\nu_4}, p_5^{\nu_5}, p_6^{\nu_6}, q_4).$$

where the semi-colon indicates that particle 4 is in the same kinematic region as particles 1 and 2.

4.1 $A^{ggg(0)}(p_4^+; p_5^+, p_6^+)$

As discussed, the simplest amplitudes are Maximally Helicity-Violating (MHV) and contain exactly two gluons with helicity opposite to the rest. It follows that the simplest helicity configuration of the Central-emission Vertex can be obtained from an MHV amplitude.

The $A^{ggg(0)}(+; +, +)$ CEV configuration can be obtained from the A-type MHV:

$$M_{7g}(p_1^-, p_2^-, p_3^+, p_4^+, p_5^+, p_6^+, p_7^+)$$

This is evaluated using the Parke-Taylor formula for an MHV where the majority of particles are positive helicity.

$$M_{7g} = \frac{\langle 12 \rangle^4}{\langle 12 \rangle \langle 23 \rangle \langle 34 \rangle \langle 45 \rangle \langle 56 \rangle \langle 67 \rangle \langle 71 \rangle}.$$

The B-type configuration is obtained by swapping particles 2 and 4.

$$M_{7g}^{\mathbf{I}} = \frac{\langle 14 \rangle^4}{\langle 14 \rangle \langle 43 \rangle \langle 32 \rangle \langle 25 \rangle \langle 56 \rangle \langle 67 \rangle \langle 71 \rangle}. \quad (88)$$

This is expanded in light-cone components by using the spinor-product identities.

$$M_{7g}^{\mathbf{I}} = \frac{-p_3^+ p_5^+ (p_3^- + p_4^- + p_5^- + p_6^- + p_7^-) (p_3^+ + p_4^+ + p_5^+ + p_6^+ + p_7^+)}{p_{3\perp} p_{5\perp} \left(p_{3\perp} \sqrt{\frac{p_4^+}{p_3^+}} - p_{4\perp} \sqrt{\frac{p_3^+}{p_4^+}} \right) \sqrt{p_3^+ p_4^+ p_5^+ p_6^+ p_7^+} \left(p_{5\perp} \sqrt{\frac{p_6^+}{p_5^+}} - p_{6\perp} \sqrt{\frac{p_5^+}{p_6^+}} \right) \left(p_{6\perp} \sqrt{\frac{p_7^+}{p_6^+}} - p_{7\perp} \sqrt{\frac{p_6^+}{p_7^+}} \right)} \quad (89)$$

In order to take the NNMRK limit of this expression, we parameterise the components:

$$\begin{aligned} p_3^+ &\rightarrow \frac{1}{\lambda} p_3^+, & p_7^+ &\rightarrow \lambda p_7^+ \\ p_3^- &\rightarrow \lambda p_3^-, & p_7^- &\rightarrow \frac{1}{\lambda} p_7^- \end{aligned} \quad (90)$$

The NNMRK limit is then the limit $\lambda \rightarrow 0$.

$$M_{7g}^{\mathbf{I}} \Big|_{\text{NNMRK}} = \frac{p_3^+ p_5^+ p_7^-}{p_{3\perp} p_{4\perp} p_{5\perp} p_{7\perp} (p_5^+ p_{6\perp} - p_6^+ p_{5\perp}) \lambda^2} \quad (91)$$

This can be expressed in terms of minimal variables.

$$M_{7g}^{\mathbf{I}} \Big|_{\text{NNMRK}} = -\frac{sY(z_1 + 1)(z_2 - 1)^2(z_3 - 1)^2 q_{1\perp}^* q_{4\perp}^*}{q_{1\perp} q_{4\perp}^2 z_3 (Y(z_2 - 1) - z_3) t_1 t_4} \quad (92)$$

It is now possible to extract the CEV using Equation 79.

$$A^{ggg(0)}(+; +, +) = -\frac{q_{1\perp}^*}{q_{1\perp}} \frac{Y(z_1 + 1)(z_2 - 1)^2(z_3 - 1)^2}{q_{4\perp} z_3 (Y(z_2 - 1) - z_3)} \quad (93)$$

Here $q_{1\perp}^*/q_{1\perp}$ remains a phase. There is a factor of $q_{4\perp}$ in the denominator which we would expect for dimensional reasons as the minimal variables are dimensionless but the 7pt CEV should have dimensions of inverse momentum.

It is obvious that all other CEV helicity configurations will be generated from NMHV amplitudes, since we require that p_1 and p_2 convert into particles of different helicity. The remaining helicity configurations are significantly more complicated to evaluate. NMHV amplitudes can be generated from the BCFW recursion relation (Equation 37) and have already been calculated in the spinor-helicity form in Bern et al. [26].

4.2 $A^{ggg(0)}(p_4^-; p_5^+, p_6^+)$

The next most simple CEV is $A^{ggg(0)}(p_4^-; p_5^+, p_6^+)$. This can be obtained from the expression in Section A of Bern et al. [26], which for conciseness has been converted to the notation of Section 2.2.

$$A_{\text{tree}}(p_1^-, p_2^-, p_3^-, p_4^+, p_5^+, p_6^+, p_7^+) = c_{347}^{(A)} + c_{347}^{(A)} \Big|_{\text{flip}} + c_{\text{B}}^{(A)} \quad (94)$$

A ‘flip’ operation is defined by $X|_{\text{flip}} = -X(1 \leftrightarrow 3, 4 \leftrightarrow 7, 5 \leftrightarrow 6)$. The coefficients are:

$$c_{347}^{(A)} = \frac{[4|(2+3)|1\rangle^3}{s_{234}[23][34]\langle 56\rangle\langle 67\rangle\langle 71\rangle[2|(3+4)|5\rangle} \quad (95)$$

$$c_B^{(A)} = \frac{-\langle 3|(4+5)(6+7)|1\rangle^3}{s_{345}s_{671}\langle 34\rangle\langle 45\rangle\langle 67\rangle\langle 71\rangle[2|(3+4)|5\rangle[2|(7+1)|6\rangle]}. \quad (96)$$

Following the methods above, the CEV is

$$A^{ggg(0)}(p_4^-; p_5^+, p_6^+) = R_1 + R_2 + R_3. \quad (97)$$

$$R_1 = - \frac{X^2 Y^3 z_1(z_1+1)z_1^{*3}(z_2-1)^2(z_3-1)^2}{q_{4\perp} z_3(Y(z_2-1)-z_3)(XY|z_1|^2+Y+1)(z_1(Y(Xz_1^*+z_2-1)-1)+Yz_2)}$$

$$R_2 = - \left(Y z_1^*(z_1^*+1)z_2^*|z_2-1|^2|z_3-1|^2(z_1(z_2-1)(z_3-1)+z_2z_3)^3 \right) / \\ \left(q_{4\perp} z_3(Y(z_2-1)-z_3)(X|z_1|^2(Y|z_2-1|^2+z_3)+z_2^*(z_1(z_2-1)(z_3-1)+z_2z_3)) \right. \\ \left. (|z_1|^2(XY|z_2-1|^2+X|z_3|^2+|z_2-1|^2|z_3-1|^2)+z_1z_2^*(z_2-1)(z_3-1)z_3^* \right. \\ \left. + z_1^*z_2z_3(z_2^*-1)(z_3^*-1)+|z_2|^2|z_3|^2) \right)$$

$$R_3 = - \left(X^2 Y |z_1|^2 z_1^{*2}(z_1^*+1)(z_2-1)^2(z_3-1)^2(Yz_1|z_2-1|^2+Yz_2(z_2^*-1)+z_1)^3 \right) / \\ \left(q_{4\perp} z_3(z_1(Y(Xz_1^*+z_2-1)-1)+Yz_2)(X|z_1|^2(Y|z_2-1|^2)+1)+|z_2|^2 \right) \\ \left(z_1(Yz_1^*(X+|z_2-1|^2)+Y(z_2-1)z_2^*+z_1^*)+Yz_2(z_1^*(z_2^*-1)+z_2^*) \right) \\ \left(X|z_1|^2(Y|z_2-1|^2+z_3)+z_2^*(z_1(z_2-1)(z_3-1)+z_2z_3) \right)$$

It is noted that the expression is significantly more complicated compared to the last configuration. The $(+;+,+)$ CEV has additional symmetry which simplifies it greatly. The factor of $1/q_{4\perp}$ is present as expected from dimensional analysis.

4.3 $A^{ggg(0)}(p_4^+; p_5^-, p_6^+)$

This configuration is significantly more complicated than the previous one because partons of the same helicity are not adjacent. This configuration was generated from the B-type colour ordering of Section D of Bern et al. [26].

$$A_{\text{tree}}(p_1^-, p_2^+, p_3^-, p_4^+, p_5^-, p_6^+, p_7^+) = c_{257}^{(D)} + c_{347}^{(D)} + c_B^{(D)} + c_{256}^{(D)} + c_B^{(D)} \Big|_{\text{flip}} + c_{256}^{(D)} \Big|_{\text{flip}} \quad (98)$$

The flip operation is different to the previous amplitude and is defined by

$$X|_{\text{flip}} = -X(1 \leftrightarrow 5, 2 \leftrightarrow 4, 6 \leftrightarrow 7).$$

The coefficients are:

$$c_{257}^{(D)} = \frac{\langle 13 \rangle^4 \langle 35 \rangle^4 [67]^3}{\langle 12 \rangle \langle 23 \rangle \langle 34 \rangle \langle 45 \rangle [6|(4+5)|3][7|(1+2)|3]} \quad (99)$$

$$\times \frac{1}{\langle 3|(4+5)(6+7)|1 \rangle \langle 3|(1+2)(6+7)|5 \rangle} \quad (100)$$

$$c_{347}^{(D)} = \frac{[24]^4 \langle 15 \rangle^4}{s_{345} [23][34] \langle 56 \rangle \langle 67 \rangle \langle 71 \rangle [2|(3+4)|5][4|(2+3)|1]} \quad (101)$$

$$c_B^{(D)} = \frac{\langle 13 \rangle^4 [4|(6+7)|5]^4}{s_{123} s_{567} \langle 12 \rangle \langle 23 \rangle \langle 56 \rangle \langle 67 \rangle [4|(5+6)|7][4|(2+3)|1] \langle 3|(1+2)(6+7)|5]} \quad (102)$$

$$c_{256}^{(D)} = \frac{\langle 13 \rangle^4 [46]^4}{s_{456} \langle 12 \rangle \langle 23 \rangle [45][56] \langle 71 \rangle [4|(5+6)|7][6|(4+5)|3]}. \quad (103)$$

The coefficients are expanded using the spinor-helicity expressions, the NNMRK limit is taken, the result is expressed in terms of the minimal set and the CEV is extracted. The expression for this helicity configuration is:

$$A^{gg(0)}(p_4^+; p_5^-, p_6^+) = P_1 + P_2 + P_3 + P_4 + P_5 + P_6 \quad (104)$$

$$P_1 = - \left(Y z_1^5 z_2^* (z_1^* + 1) (z_2 - 1) (z_3 - 1) |z_2 - 1|^2 |z_3 - 1|^2 \right) / \\ \left(q_{4\perp} z_1^* z_2 z_3 (Y(z_1 + 1) z_2 - (Y + 1) z_1) (z_1(z_2 - 1)(z_3 - 1) + z_2 z_3) \right. \\ \left. (Y z_1 |z_2 - 1|^2 + Y z_2 (z_2^* - 1) + z_1) (Y(z_2^* - 1)(z_1(z_2 - 1) + z_2) + z_1 z_3^*) \right)$$

$$P_2 = \frac{Y^3 z_1 (z_1 + 1) (z_2 - 1)^2 (z_3 - 1)^2}{q_{4\perp} z_1^* z_3 (Y(1 - z_2) + z_3) (XY |z_1|^2 + Y + 1) (z_1 (Y(X z_1^* + z_2 - 1) - 1) + Y z_2)}$$

$$P_3 = - \frac{Y^3 z_1 (z_2 - 1) (z_3 - 1) |z_1 + 1|^2 |z_2 - 1|^2 |z_3 - 1|^2}{q_{4\perp} (Y + 1) z_1^* z_3 (z_2^* + z_3^* - 1) (Y(z_1 + 1) z_2 - (Y + 1) z_1) (Y(z_2 - 1) - z_3)}$$

$$P_4 = \frac{Y^3 z_1 (z_1 + 1) (z_1^* + 1) (z_2 - 1)^2 (z_2^* - 1)^4 z_2^* (z_3 - 1)^2}{q_{4\perp} z_1^* z_3 (z_2^* + z_3^* - 1) (Y(1 - z_2^*) + z_3^*) \left(Y(z_2^* - 1) (z_1(z_2 - 1) + z_2) + z_1 z_3^* \right) (Y |z_2 - 1|^2 + |z_3|^2)}$$

$$\begin{aligned}
P_5 = & - \left(Y z_1^5 (z_1^* + 1) (z_2 - 1)^2 (z_3 - 1)^2 (z_2^* - XY z_1^* (z_2^* - 1))^4 \right) / \\
& \left(q_{4\perp} z_1^* z_3 (Y z_1 |z_2 - 1|^2 + Y z_2 (z_2^* - 1) + z_1) (z_1 (Y (X z_1^* + z_2 - 1) - 1) + Y z_2) \right. \\
& (X |z_1|^2 (Y |z_2 - 1|^2 + 1) + |z_2|^2) \\
& (|z_1|^2 (XY + Y + 1) + Y (z_1^* + 1) z_2^* (z_1 (z_2 - 1) + z_2) - Y (z_1 + 1) z_1^* z_2) \\
& \left. (X |z_1|^2 (Y |z_2 - 1|^2 + z_3) + z_2^* (z_1 (z_2 - 1) (z_3 - 1) + z_2 z_3)) \right)
\end{aligned}$$

$$\begin{aligned}
P_6 = & - \left(X^2 Y z_1^2 z_2^* z_3^3 (z_1^* + 1) |z_1|^2 |z_2 - 1|^2 |z_3 - 1|^2 \right) / \\
& \left(q_{4\perp} (Y (z_2 - 1) - z_3) (z_1 (z_2 - 1) (z_3 - 1) + z_2 z_3) \right. \\
& (X |z_1|^2 (Y |z_2 - 1|^2 + z_3) + z_2^* (z_1 (z_2 - 1) (z_3 - 1) + z_2 z_3)) \\
& \left(|z_1|^2 (XY |z_2 - 1|^2 + X |z_3|^2 + |z_2 - 1|^2 |z_3 - 1|^2) + z_1 z_2^* z_3^* (z_2 - 1) (z_3 - 1) + \right. \\
& \left. \left. + z_1^* z_2 (z_2^* - 1) z_3 (z_3^* - 1) + |z_2|^2 |z_3|^2 \right) \right)
\end{aligned}$$

4.4 $A^{ggg(0)}(p_4^+; p_5^+, p_6^-)$

This configuration was generated from the reflected B-type colour-ordering (as in Equation 53) of Section B in Bern et al. [26]'s paper. This amplitude is unique in not possessing any flip symmetry.

$$A_{\text{tree}}(p_1^-, p_2^-, p_3^+, p_4^-, p_5^+, p_6^+, p_7^+) = c_B^{(B)} + c_C^{(B)} + c_{125}^{(B)} + c_{347}^{(B)} + c_{357}^{(B)}. \quad (105)$$

The coefficients are:

$$c_B^{(B)} = \frac{\langle 12 \rangle^3 [7] (5+6) |4\rangle^3}{s_{123} s_{456} \langle 23 \rangle \langle 45 \rangle \langle 56 \rangle [7] (1+2) |3\rangle \langle 6 | (4+5) (2+3) |1\rangle} \quad (106)$$

$$c_C^{(B)} = \frac{-\langle 4 | (3+5) (6+7) |1\rangle^4}{s_{345} s_{167} \langle 34 \rangle \langle 45 \rangle \langle 67 \rangle \langle 71 \rangle [2] (3+4) |5\rangle [2] (7+1) |6\rangle \langle 3 | (4+5) (6+7) |1\rangle} \quad (107)$$

$$c_{125}^{(B)} = \frac{[7] (1+2) |4\rangle^4}{s_{127} [12] \langle 34 \rangle \langle 45 \rangle \langle 56 \rangle [71] [2] (7+1) |6\rangle [7] (1+2) |3\rangle} \quad (108)$$

$$c_{347}^{(B)} = \frac{[3] (2+4) |1\rangle^4}{s_{234} [23] [34] \langle 56 \rangle \langle 67 \rangle \langle 71 \rangle [2] (3+4) |5\rangle [4] (2+3) |1\rangle} \quad (109)$$

$$c_{357}^{(B)} = \frac{\langle 12 \rangle^3 [5] (6+7) |1\rangle^3}{\langle 23 \rangle [45] \langle 67 \rangle \langle 71 \rangle [4] (2+3) |1\rangle} \quad (110)$$

$$\times \frac{1}{\langle 3 | (4+5) (6+7) |1\rangle \langle 6 | (4+5) (2+3) |1\rangle}. \quad (111)$$

The expression for this helicity configuration is

$$A^{ggg(0)}(p_4^+, p_5^+, p_6^-) = Q_1 + Q_2 + Q_3 + Q_4 + Q_5. \quad (112)$$

$$\begin{aligned}
Q_1 = & - (X^2 Y^3 z_1^2 |z_1|^2 (z_1^* + 1)(z_2 - 1) |z_2 - 1|^2 (z_3 - 1)^2 (z_3^* - 1)) / \\
& \left(q_{4\perp} z_3 (Y + 1) (Y(z_2 - 1) - 1) (Y(z_2 - 1) - z_3) (XY |z_1|^2 + Y + 1) \right. \\
& \left. (z_1^* (XY z_1 (z_2^* + z_3^* - 1) + Y(z_2^* - 1)(z_3^* - 1) + (z_2^* - 1)(z_3^* - 1)) + (Y + 1) z_2^* z_3^*) \right) \\
Q_2 = & - \left(Y^3 z_1 (z_1^* + 1) (z_2 - 1)^2 z_2^* (z_3 - 1)^2 (|z_1|^2 (X z_3^* + z_2 (z_2^* - 1)(z_3^* - 1) - z_2^* z_3^* + z_2^* + z_3^* - 1) \right. \\
& \left. + z_1 (z_2 - 1) z_2^* z_3^* + z_1^* z_2 (z_2^* - 1)(z_3^* - 1) + |z_2|^2 z_3^*)^4 \right) / \\
& \left(q_{4\perp} z_1^* z_3 (Y(z_2^* - 1)(z_1(z_2 - 1) + z_2) + z_1 z_3^*) (z_1 (Y z_1^* (X + |z_2 - 1|^2) + \right. \\
& \left. + Y(z_2 - 1) z_2^* + z_1^*) + Y z_2 (z_1^* (z_2^* - 1) + z_2^*)) (X |z_1|^2 (Y |z_2 - 1|^2 + z_3^*) \right. \\
& \left. + z_2 (z_1^* (z_2^* - 1)(z_3^* - 1) + z_2^* z_3^*)) \right. \\
& \left(|z_1|^2 (XY (z_2^* + z_3^* - 1) + Y |z_2 - 1|^2 (z_3^* - 1) - z_2^* z_3^* + z_2^* + z_3^* - 1) + \right. \\
& \left. + z_1 z_2^* z_3^* (Y(z_2 - 1) - 1) + Y z_1^* z_2 (z_2^* - 1)(z_3^* - 1) + Y |z_2|^2 z_3^*) \right. \\
& \left. (|z_1|^2 (XY |z_2 - 1|^2 + X |z_3|^2 + |z_2 - 1|^2 |z_3 - 1|^2) \right. \\
& \left. + z_1 (z_2 - 1) z_2^* (z_3 - 1) z_3^* + z_1^* z_2 (z_2^* - 1) z_3 (z_3^* - 1) + z_2 z_2^* z_3 z_3^*) \right) \\
Q_3 = & - (X^2 Y^3 z_1^2 z_2^* |z_1|^2 (z_1^* + 1) (z_2 - 1)^4 |z_2 - 1|^2 |z_3 - 1|^2) / \\
& \left(q_{4\perp} z_2 z_3 (Y(z_2 - 1) - 1) (X |z_1|^2 (Y |z_2 - 1|^2 + 1) + |z_2|^2) \right. \\
& \left. (X |z_1|^2 (Y |z_2 - 1|^2 + z_3^*) + z_2 (z_1^* (z_2^* - 1)(z_3^* - 1) + z_2^* z_3^*)) \right) \\
Q_4 = & (Y z_1 z_2^* (z_3^*)^4 |z_1 + 1|^2 (z_2 - 1)^2 (z_3 - 1)^2) / \\
& \left(q_{4\perp} z_1^* z_3 (z_2^* + z_3^* - 1) (Y(1 - z_2^*) + z_3^*) (Y(z_2^* - 1)(z_1(z_2 - 1) + z_2) + z_1 z_3^*) (Y |z_2 - 1|^2 + |z_3|^2) \right)
\end{aligned}$$

$$\begin{aligned}
Q_5 = & - (Y z_1 (z_1 + 1) (z_2 - 1)^2 (z_3 - 1)^2 (z_1^* (z_2^* - 1) (z_3^* - 1) + z_2^* z_3^*)^3) / \\
& \left(q_{4\perp} z_1^* z_3 (z_2^* + z_3^* - 1) (Y (z_2 - 1) - z_3) \left(z_1^* (X Y z_1 (z_2^* + z_3^* - 1) + Y (z_2^* - 1) (z_3^* - 1) + (z_2^* - 1) (z_3^* - 1)) \right. \right. \\
& \quad \left. \left. + (Y + 1) z_2^* z_3^* \right) (z_1 z_3^* (Y z_1^* (X - z_2 + 1) + (z_1^* + 1) z_2^* (Y (z_2 - 1) - 1) + z_1^*) + |z_1|^2 (z_2^* - 1) \right. \\
& \quad \left. \left. (Y (X - z_2 + 1) + 1) + Y z_2 (z_1^* (z_2^* - 1) (z_3^* - 1) + z_2^* z_3^*) \right) \right)
\end{aligned}$$

5 Analysis

The results presented in the previous section are novel and therefore cannot be compared with any published work. In order to have confidence that the results are correct, they are subjected to a series of independent checks.

5.1 Numerical check

The most basic method for checking the accuracy of the results is to substitute numerical values for each of the components and compare the general literature result (for example Equation 88) to the final amplitude after the NNMRK limit (Equation 92). The numerical values must satisfy momentum conservation at each vertex as well as the on-shell condition $p_i^+ p_i^- = |p_{i\perp}|^2$. The literature result is parameterised as in Equation 90 and a ratio is taken between it and the final result. As $\lambda \rightarrow 0$ this value should approach unity. All results pass a numerical check.

5.2 NMRK and MRK limits

In NNMRK no hierarchy is assumed between central particles. If we introduce a hierarchy such that one of the central particles has longitudinal momentum much greater (or less than) the other two this becomes the NMRK limit. In this limit, all ‘interaction’ (cross) terms between the particles of different momenta scales are suppressed and the 3-CEV factorises into the product of a 1-CEV and a 2-CEV, connected by a propagator. This is frequently used to check that results are correct [6, 20].

In the NMRK limit $p_4^+ \gg p_5^+, p_6^+$, the propagator is $1/t_2 = -|q_{2\perp}|^2$. This limit is particularly simple in terms of minimal variables:

$$X = \frac{p_4^+}{p_5^+} \rightarrow \infty, \quad Y = \frac{p_5^+}{p_6^+} \rightarrow Y \quad (113)$$

In scaling X we take $p_4^+ \gg p_5^+$, by not scaling Y , we keep p_5^+ and p_6^+ of the same order thus fulfilling the conditions for an NMRK limit. We choose to isolate p_4 because this allows us

to compare to literature results in A-type colour ordering. The difference between A and B-type in terms of the single-gluon CEV is that p_4 , is in the ‘incoming region’. This is obvious from Figure 5 in Section 3.4. If p_4 is separated into a 1-CEV, the only difference is the presence of an additional minus sign. The 2-CEV of p_5 and p_6 is then identical to A-type. While we are free to instead separate p_6 from p_4 and p_5 , this would not allow a comparison to the A-type configurations calculated in Byrne et al. [20].

The four results are checked in the NMRK and MRK limits. If it has already been shown that a given two-gluon CEV factorises correctly in the MRK limit, only an NMRK check will be demonstrated.

5.2.1 $A^{ggg(0)}(p_4^+, p_5^+, p_6^+)$ check

In the limit $X \rightarrow \infty$ Equation (93) remains the same since it has no X dependence:

$$A_{\text{NMRK}}^{ggg(0)}(+; +, +) = -\frac{q_{1\perp}^* Y(z_1 + 1)(z_2 - 1)^2(z_3 - 1)^2}{q_{1\perp} q_{4\perp} z_3 (Y(z_2 - 1) - z_3)} \quad (114)$$

The 1-CEV corresponding to p_4 has been calculated in an A-type colour-ordering in Byrne et al. [20]. In B-type this has an additional minus sign.

$$A_{\text{B-type}}^{g(0)}(q_1, p_4^+, q_2) = -\frac{q_{1\perp}^* q_{2\perp}}{p_{4\perp}} \quad (115)$$

Then dividing the 3-CEV by the 1-CEV corresponding to p_4 and the propagator $1/t_2$ will leave the 2-CEV corresponding to p_5^+ and p_6^+ : $A^{gg(0)}(p_4^+, p_5^+)$.

$$\left(-\frac{q_{1\perp}^* Y(z_1 + 1)(z_2 - 1)^2(z_3 - 1)^2}{q_{1\perp} q_{4\perp} z_3 (Y(z_2 - 1) - z_3)} \right) \left(-\frac{p_{4\perp}}{q_{1\perp}^* q_{2\perp}} \right) (t_2) = -\frac{q_{2\perp}^* Y z_2 (z_2 - 1)(z_3 - 1)}{q_{2\perp} (Y(z_2 - 1) - z_3)} \quad (116)$$

We have converted $p_{4\perp}$ into minimal variables and expressed the result in terms of $q_{2\perp}$. To compare to the literature result [20] we need to change variables to account for two things. Firstly, ‘position’ of the 2-CEV is under the 1-CEV and secondly, the different minimal variables convention in Byrne et al. [20]. This compound substitution is

$$Y \rightarrow X, \quad q_{2\perp} \rightarrow q_{1\perp}, \quad z_2 \rightarrow 1 - z, \quad z_3 \rightarrow w, \quad (117)$$

which results in:

$$\frac{q_{1\perp}^*}{q_{1\perp}} \frac{z(w - 1)(z - 1)X}{(w + Xz)}. \quad (118)$$

This is the expression for the 2-CEV $A^{gg(0)}(q_1, p_4^+, p_5^+, q_3)$ as derived in Appendix A and is in agreement with Byrne et al. [20].

We can take the MRK limit of Equation (114) by taking $Y \rightarrow \infty$,

$$A_{\text{MRK}}^{ggg(0)}(+; +, +) = -\frac{q_{1\perp}^* (z_1 + 1)(z_2 - 1)(z_3 - 1)^2}{q_{1\perp} q_{4\perp} z_3}. \quad (119)$$

We expect this to factorise into the product of three 1-CEVs corresponding to each of the central particles, and two propagators: $1/t_2$, $1/t_3$. Note again that a minus sign arises in the p_4 case from the colour ordering,

$$p_4 : -\frac{q_{1\perp}^* q_{2\perp}}{p_{4\perp}} \quad p_5 : \frac{q_{2\perp}^* q_{3\perp}}{p_{5\perp}} \quad p_6 : \frac{q_{3\perp}^* q_{4\perp}}{p_{6\perp}}. \quad (120)$$

Dividing Equation (119) by the 1-CEVs above gives:

$$\frac{1}{q_{2\perp} q_{2\perp}^* q_{3\perp} q_{3\perp}^*} \quad (121)$$

which is the product of the two propagators as expected. Therefore $A^{ggg(0)}(p_4^+; p_5^+, p_6^+)$ passes the MRK and NMRK checks.

5.2.2 $A^{ggg(0)}(p_4^-; p_5^+, p_6^+)$ check

Following the same method as above, the NMRK limit of $A^{ggg(0)}(p_4^-; p_5^+, p_6^+)$ (Equation 97) is found by taking the limit $X \rightarrow \infty$.

$$A_{\text{NMRK}}^{ggg(0)}(p_4^-; p_5^+, p_6^+) = -\frac{Y z_1^* (z_1 + 1) (z_2 - 1)^2 (z_3 - 1)^2}{q_{4\perp} z_1 z_3 (Y (z_2 - 1) - z_3)} \quad (122)$$

Dividing this by the propagator $1/t_2$ and the conjugate of Equation (115) (the helicity of p_4 is negative), we have:

$$A_{\text{NMRK}}^{ggg(0)}(p_4^-; p_5^+, p_6^+) \left(-\frac{p_{4\perp}^*}{q_{1\perp} q_{2\perp}^*} \right) (t_2) = -\frac{q_{2\perp}^* Y z_2 (z_2 - 1) (z_3 - 1)}{q_{2\perp} (Y (z_2 - 1) - z_3)} \quad (123)$$

Which is identical to Equation (116). This was shown to factorise into two 1-CEVs in the MRK limit. Therefore this configuration passes the MRK and NMRK checks.

5.2.3 $A^{ggg(0)}(p_4^+; p_5^-, p_6^+)$ check

It was not possible to analytically transform the result in the NMRK limit into a comparable result due to the complexity of this configuration. However the NMRK result was checked numerically and found to be in agreement with literature. While this is considered to pass the NMRK check, further investigation is required to have complete confidence in this result. The MRK limit is simpler and it was possible to make an analytic comparison.

The $A^{ggg(0)}(p_4^+; p_5^-, p_6^+)$ result is checked in the MRK limit

$$X \rightarrow \infty, \quad Y \rightarrow \infty.$$

The MRK limit is:

$$A_{\text{MRK}}^{ggg(0)}(p_4^+; p_5^-, p_6^+) = -\frac{z_1 (z_1^* + 1) (z_2^* - 1) (z_3 - 1)^2}{q_{4\perp} z_1^* z_3} \quad (124)$$

The 1-CEVs corresponding to p_4^+ , p_5^- and p_6^+ in a B-type colour ordering (which introduces a negative sign for the CEV corresponding to p_4) are respectively:

$$p_4 : -\frac{q_{1\perp}^* q_{2\perp}}{p_{4\perp}} \quad p_5 : \frac{q_{2\perp} q_{3\perp}^*}{p_{5\perp}^*} \quad p_6 : \frac{q_{3\perp}^* q_{4\perp}}{p_{6\perp}}. \quad (125)$$

Dividing Equation 124 by the three expressions for the 1-CEVs above and converting to minimal variables leaves us with:

$$\frac{1}{q_{2\perp} q_{2\perp}^* q_{3\perp} q_{3\perp}^*} \quad (126)$$

which again is the product of the two propagators as expected.

5.2.4 $A^{ggg(0)}(p_4^+, p_5^+, p_6^-)$ check

The NMRK limit of $A^{ggg(0)}(p_4^+, p_5^+, p_6^-)$ (Equation 112) is:

$$\begin{aligned} A_{\text{NMRK}}^{ggg(0)}(p_4^+, p_5^+, p_6^-) &= \frac{Y z_1 (z_1^* + 1) (z_2 - 1)^2 (z_3 - 1)}{q_{4\perp} z_1^* z_3} \times \\ &\left(-\frac{Y^2 (z_2 - 1)^3 (z_2^* - 1) z_2^* (z_3^* - 1)}{z_2 (Y(z_2 - 1) - 1) (Y(z_2 - 1) (z_2^* - 1) + 1) (Y(z_2 - 1) (z_2^* - 1) + z_3^*)} \right. \\ &\quad - \frac{z_2^* (z_3 - 1) (z_3^*)^4}{(z_2^* + z_3^* - 1) (Y(z_2 - 1) (z_2^* - 1) + z_3^*) (Y(z_2^* - 1) (z_1 (z_2 - 1) + z_2) + z_1 z_3^*) (Y(z_2 - 1) (z_2^* - 1) + z_3 z_3^*)} \\ &\quad + \frac{(z_1 + 1) z_2^* (z_3 - 1) (z_3^*)^4}{(z_2^* + z_3^* - 1) (Y(-z_2^*) + Y + z_3^*) (Y(z_2^* - 1) (z_1 (z_2 - 1) + z_2) + z_1 z_3^*) (Y(z_2 - 1) (z_2^* - 1) + z_3 z_3^*)} \\ &\quad \left. - \frac{(z_2^* - 1) (z_3 - 1) (z_3^* - 1)}{(Y + 1) (Y(z_2 - 1) - 1) (z_2^* + z_3^* - 1) (Y(z_2 - 1) - z_3)} \right) \end{aligned}$$

The 1-CEV associated to p_4^+ in a B-type ordering is

$$-\frac{q_{1\perp}^* q_{2\perp}}{p_{4\perp}} \quad (127)$$

Dividing the 3-CEV by the 1-CEV and the propagator $1/t_2$ we should be left with the opposite helicity 2-CEV.

$$A_{\text{NMRK}}^{ggg(0)}(p_4^+, p_5^+, p_6^-) \left(-\frac{q_{1\perp}^* q_{2\perp}}{p_{4\perp}} \right) (t_2) = \quad (128)$$

$$X(1 - z) z \left(\frac{(w - 1)(w^* - 1) z^*}{(X + 1)(w^* - z^*)(Xz + 1)(w + Xz)} + \quad (129)$$

$$\frac{(w^* - 1) X^2 z^3 (z^* - 1) z^*}{(z - 1)(Xz + 1)(Xz z^* + 1)(w^* + Xz z^*)} \right) + \quad (130)$$

$$\frac{(w - 1) w^{*4} X (z - 1) z (z^* - 1)}{(w^* - z^*)(w^* + Xz^*)(w^* + Xz z^*)(w w^* + Xz z^*)} \quad (131)$$

Which is in agreement with Equation 3.25 in Byrne et al. [20]. This is an alternative representation to Equation 151 (in this report), therefore this configuration passes the MRK and NMRK checks.

5.3 Soft check

We can use the Soft Limit discussed in Section 2.3.3 to check the consistency of the results. The soft gluon must be central and it is easiest to take $p_4 \rightarrow 0$ so that results can be easily compared to A-type colour ordered expressions.

5.3.1 Extraction of the two-gluon, same helicity CEV

In the limit that p_4 is soft, $A^{gg(0)}(+; +, +)$ and $A^{gg(0)}(-; +, +)$ should decay into the product of $A^{gg(0)}(q_{1\perp}, p_4^+, p_5^+, q_{3\perp})$ (Appendix A, Equation 148) and an eikonal factor.

Consider $A^{gg(0)}(-; +, +)$ (Equation 97). Noting the impact of the colour-ordering, the eikonal factor corresponding to p_4^- in general kinematics is

$$S(1, p_4^-, 3) = \frac{[31]}{[34][41]} = \frac{\sqrt{p_3^+(p_3^- + p_4^- + p_5^- + p_6^- + p_7^-)}}{\left(p_{4\perp}^* \sqrt{\frac{p_3^+}{p_4^+}} - p_{3\perp}^* \sqrt{\frac{p_4^+}{p_3^+}}\right) \sqrt{p_4^+(p_3^- + p_4^- + p_5^- + p_6^- + p_7^-)}}.$$

The NNMRK limit of the soft factor is taken so that the kinematics of the eikonal factor are consistent with the expression for the CEV. As usual, the limit is taken using the parameterisation of Equation 90,

$$S(p_1, p_4^-, p_3)_{\text{NNMRK}} = \frac{1}{p_{4\perp}^*} = \frac{1 + z_1^*}{q_{1\perp}^*}, \quad (132)$$

which approaches infinity as $p_4 \rightarrow 0$. Again, we note that the eikonal factor does not depend on the helicities of particles 1 and 3.

The expression for $A^{gg(0)}(p_4^-; p_5^+, p_6^+)$ (Equation 97) is divided by the soft factor. In order to take the soft limit that $p_4 \rightarrow 0$ the components of p_4 must be scaled equally in the expression for the CEV such that quantities like $p_{4\perp}/p_4^+$ remain finite.

The minimal variables are parameterised as:

$$X \rightarrow \epsilon X, \quad z_1 \rightarrow \frac{z_1}{\epsilon}. \quad (133)$$

Now, the limit $\epsilon \rightarrow 0$ is taken,

$$\frac{A^{gg(0)}(p_4^-; p_5^+, p_6^+)}{S(p_1, p_4^-, p_3)_{\text{NNMRK}}} = -\frac{q_{2\perp}^* Y(z_2 - 1) z_2 (z_3 - 1)}{q_{2\perp} (Y(z_2 - 1) - z_3)}. \quad (134)$$

This is identical to Equation 116 which was shown to be in agreement with Byrne et al. [20].

Following this analysis for $A^{gg(0)}(p_4^+; p_5^+, p_6^+)$ (Equation 93) we find the eikonal factor corresponding to p_4^+ is

$$S(p_1, p_4^+, p_3)_{\text{NNMRK}} = -\frac{1}{p_{4\perp}} = -\frac{1 + z_1}{q_{1\perp}}. \quad (135)$$

This is the conjugate of Equation 132. It is found that

$$\frac{A^{ggg(0)}(p_4^+; p_5^+, p_6^+)}{S(p_1, p_4^+, p_3)_{\text{NNMRK}}} = -\frac{q_{2\perp}^* Y(z_2 - 1) z_2 (z_3 - 1)}{q_{2\perp} (Y(z_2 - 1) - z_3)} \quad (136)$$

which is identical to Equation 116 and 134. Therefore $A^{ggg(0)}(p_4^+; p_5^+, p_6^+)$ and $A^{ggg(0)}(p_4^-; p_5^+, p_6^+)$ both pass the soft check.

5.3.2 Extraction of the two-gluon, opposite helicity CEV

In the limit that p_4 is soft, $A^{ggg(0)}(p_4^+; p_5^-, p_6^+)$ and $A^{ggg(0)}(p_4^+; p_5^+, p_6^-)$ are expected to decay to the product of an eikonal factor and the opposite helicity 2-CEV: $A^{gg(0)}(q_{1\perp}, p_4^\pm, p_5^\mp, q_{3\perp})$ (Equation 151).

The above steps are repeated for $A^{ggg(0)}(p_4^+; p_5^+, p_6^-)$. The eikonal factor is Equation 135. It is found that

$$\frac{A^{ggg(0)}(p_4^+; p_5^+, p_6^-)}{S(p_1, p_4^+, p_3)_{\text{NNMRK}}} \underset{p_4 \rightarrow 0}{=} \quad (137)$$

$$- Xz \left(\frac{(w^* - 1)X^2(z - 1)z^3(z^* - 1)z^*}{(w - z)(w + Xz)(w + Xzz^*)(ww^* + Xzz^*)} \right) \quad (138)$$

$$- \frac{(w - 1)(w^* - 1)X^2(z^* - 1)z^*}{(X + 1)(w - z)(Xz^* + 1)(w^* + Xz^*)} \quad (139)$$

$$+ \frac{w(-z) + w + z - 1}{(Xz^* + 1)(Xzz^* + 1)(w + Xzz^*)} \Big). \quad (140)$$

This is equivalent to Equation 151 and in agreement with Byrne et al. [20].

Now consider, $A^{ggg(0)}(p_4^+; p_5^-, p_6^+)$. The eikonal factor is the same as above.

$$\frac{A^{ggg(0)}(p_4^+; p_5^-, p_6^+)}{S(p_1, p_4^+, p_3)_{\text{NNMRK}}} \underset{p_4 \rightarrow 0}{=} \quad (141)$$

$$\frac{(w - 1)X^3(z - 1)z(z^* - 1)(z^*)^4}{(w^* - z^*)(w^* + Xz^*)(w^* + Xzz^*)(ww^* + Xzz^*)} \quad (142)$$

$$- \frac{(w - 1)(w^* - 1)X^3(z - 1)zz^*}{(X + 1)(w^* - z^*)(Xz + 1)(w + Xz)} \quad (143)$$

$$- \frac{(w^* - 1)X(z^* - 1)z^*}{(Xz + 1)(Xzz^* + 1)(w^* + Xzz^*)}. \quad (144)$$

By inspection, this is the conjugate of Equation 137 as expected. Therefore both results pass the soft check.

6 Discussion

In the helicity basis there are eight contributions to the three-gluon CEV. Four of these are independent and the remaining four can be generated through complex conjugation. Four

independent results were presented in Section 4, therefore a complete description of the tree-level three-gluon CEV is obtainable from the results in this report.

The results presented here are one of four ingredients needed to compute the BFKL kernel at NNLL. Currently two of these have been published [19, 20] and research into the 2-loop one-gluon CEV is ongoing. This collection of results allow (in theory) the computation of higher order corrections to the predictions of QCD. These predictions can be compared to experimental results.

All of the helicity configurations pass an NMRK, MRK and soft check providing a very large degree of confidence that they are correct. The (+;- ,+) configuration was generated from the amplitude $A_{\text{tree}}(p_1^-, p_2^+, p_3^-, p_4^+, p_5^-, p_6^+, p_7^+)$ which was the most complicated due to the lack of symmetry in adjacent helicities. The NMRK check for this CEV was verified numerically as it was not possible to manipulate the expression into the correct form. While it did pass the NMRK check numerically, it would be beneficial to confirm this with another independent check, such as the collinear check [6]. It is also possible to extract the (+;- ,+) configuration from amplitude C (instead of D) in [26], which would be another excellent way to verify this result. The other helicity configurations could also be checked in this manner, since each configuration can be generated from at least two independent amplitudes, as shown in Section 2.7. This would be interesting, as alternative representations of the results presented here may be discovered.

As discussed in Section 3.5, there are multiple ways of defining a set of suitable minimal variables. It is possible that there is an optimal choice that reduces the complexity of the results. All helicity configurations were calculated in a B-type colour ordering. Future research could compute the A-type configuration for comparison. With the collection of more results it would be easier to analyse them to find the best choice of variables.

Physical singularities arise from propagators going on-shell. Due to time constraints, the singularities of the results were not analysed, however it is known that the results contain spurious singularities which originate from ‘currents’ such as $[a|(b+c)|d]$. Spurious singularities are not physical, and should therefore cancel pairwise. The results could be presented in a more intuitive form by eliminating these spurious singularities.

It is clear that the tree-level analysis of 7-pt amplitudes is significantly more complicated than at 6-pt. If higher orders of the BFKL kernel were to be computed, an 8-pt tree-level amplitude would be required in order to extract the 4-gluon CEV. It is possible that the complexity of this amplitude will prevent it being evaluated. An alternative method to extracting CEVs from amplitudes may be to generate them using recursion [29]. The three-gluon CEV can be interpreted as a 5-pt amplitude with two off-shell legs. Current research at The University of Edinburgh is investigating the possibility of an off-shell recursion relation akin to the BCFW equation. If successful, this would allow the generation of CEVs without the need to compute higher point amplitudes. The results presented here could provide a check of such a recursion relation.

7 Conclusion

The three-gluon CEV contributes to the BFKL kernel at next-to-next-to leading logarithmic order and can be used to calculate a high-precision correction to the predictions of QCD. Analytic tree-level expressions for the four independent helicity configurations of the three-gluon Central-emission Vertex in the NNMRK limit are presented. The remaining four configurations can be generated through complex conjugation of the independent results. In the NMRK and soft limits, the one-gluon and two-gluon CEVs can be extracted from the three-gluon CEV. These lower CEVs are compared to the results published in Byrne et al. [20] and found to be in complete agreement. This provides a very large amount of confidence that the results presented here are correct.

Appendices

Note — Appendices are provided for completeness only and any content included in them will be disregarded for the purposes of assessment.

A Obtaining the two-gluon CEV

Consider the MHV 6-pt colour-stripped tree amplitude $M_{6g}^{(0)}(p_1^-, p_2^-, p_3^+, p_4^+, p_5^+, p_6^+)$. This can be evaluated using the Parke-Taylor formula (Section 35).

$$M_{6g}^{(0)}(p_1^-, p_2^-, p_3^+, p_4^+, p_5^+, p_6^+) = \frac{\langle 12 \rangle^4}{\langle 12 \rangle \langle 23 \rangle \langle 34 \rangle \langle 45 \rangle \langle 56 \rangle \langle 61 \rangle} \quad (145)$$

In the NMRK limit this is

$$-\frac{p_6^- p_3^+ p_4^+}{(p_4^+ p_{3\perp} p_{4\perp} p_{5\perp} p_{6\perp} - p_5^+ p_{3\perp} p_{4\perp}^2 p_{6\perp})} \quad (146)$$

which can be rewritten in the minimal set.

$$M_{6g}^{(0)}(p_1^-, p_2^-, p_3^+, p_4^+, p_5^+, p_6^+) \Big|_{\text{NMRK}} = -\frac{sw^2 X(z-1)^3}{(w-1)zq_{1\perp}^4(w+Xz)} \quad (147)$$

Now using Equation 79 and the results for the impact factors (equation 2.4), we can identify the CEV as

$$A^{gg(0)}(q_{1\perp}, p_4^+, p_5^+, q_{3\perp}) = M_{6g}^{(0)}(p_1^-, p_2^-, p_3^+, p_4^+, p_5^+, p_6^+) \frac{t_1 t_3}{s C^{g(0)}(p_2^-, p_3^+) C^{g(0)}(p_1^-, p_6^+)} \quad (148)$$

$$(149)$$

$$= \frac{(1-w)X(z-1)zq_{1\perp}^*}{q_{1\perp}(w+Xz)} \quad (150)$$

In agreement with Byrne 2022 ([20]). Note that $\frac{q_{1\perp}^*}{q_{1\perp}}$ remains as a phase factor.

Now consider the NMHV amplitude

$$\begin{aligned} M_{6g}^{(0)}(p_1^-, p_2^+, p_3^-, p_4^+, p_5^-, p_6^+) = & \\ & - \frac{\langle 13 \rangle^4 [46]^2}{\langle 12 \rangle \langle 23 \rangle [45] [56] s_{123} \langle 1|2+3|4 \rangle \langle 3|4+5|6 \rangle} \\ & - \frac{[24]^4 [15]^4}{[23] [34] \langle 56 \rangle \langle 61 \rangle s_{234} \langle 5|3+4|2 \rangle \langle 1|5+6|4 \rangle} \\ & - \frac{[26]^4 \langle 35 \rangle^4}{\langle 34 \rangle \langle 45 \rangle [61] [12] s_{345} \langle 3|4+5|6 \rangle \langle 5|6+1|2 \rangle} \end{aligned}$$

In the NRMK limit this becomes:

$$\begin{aligned}
M_{6g}^{(0)}(p_1^-, p_2^+, p_3^-, p_4^+, p_5^-, p_6^+) & \stackrel{=}{\text{NMRK}} \\
& - \frac{q_{3\perp}^*}{q_{3\perp}} \frac{sX^3|w-1|^2|z|^2(z^*-1)}{t_1t_3(X+1)(w-z)(Xz^*+1)(w^*+Xz^*)} \\
& - \frac{q_{3\perp}^*}{q_{3\perp}} \frac{sXz(w-1)(z-1)}{t_1t_3(X|z|^2+1)(Xz^*+1)(X|z|^2+w)} \\
& + \frac{q_{3\perp}^*}{q_{3\perp}} \frac{sX^3z^3|z-1|^2(w^*-1)|z|^2}{t_1t_3(w-z)(w+Xz)(X|z|^2+w)(|w|^2+X|z|^2)}
\end{aligned}$$

By using Equation 79 we reach:

$$\begin{aligned}
A^{gg(0)}(q_{1\perp}, p_4^+, p_5^-, q_{3\perp}) & \stackrel{=}{\text{NMRK}} \\
& - \frac{X^3|w-1|^2|z|^2(z^*-1)}{(X+1)(w-z)(Xz^*+1)(w^*+Xz^*)} \\
& - \frac{Xz(w-1)(z-1)}{(X|z|^2+1)(Xz^*+1)(X|z|^2+w)} \\
& + \frac{X^3z^3|z-1|^2(w^*-1)|z|^2}{(w-z)(w+Xz)(X|z|^2+w)(|w|^2+X|z|^2)}
\end{aligned} \tag{151}$$

In agreement with Byrne 2005 [20] (Equation 3.23) up to an overall phase factor.

B Useful expressions in minimal variables

The minimal variables are:

$$z_1 = \frac{q_{2\perp}}{p_{4\perp}} \quad z_2 = \frac{q_{2\perp}}{p_{5\perp}} \quad z_3 \equiv \frac{q_{3\perp}}{p_{6\perp}} \quad X = \frac{p_4^+}{p_5^+} \quad Y \equiv \frac{p_5^+}{p_6^+} \tag{152}$$

In order to transform from light-cone coordinates to minimal variables, the following quantities must be derived.

$$\begin{aligned}
q_{1\perp} &= q_{2\perp} + p_{4\perp} \\
&= z_1 p_{4\perp} + p_{4\perp} \\
\Rightarrow p_{4\perp} &= \frac{q_{1\perp}}{1+z_1}
\end{aligned} \tag{153}$$

$$\begin{aligned}
q_{2\perp} &= p_{5\perp} + q_{3\perp} \\
q_{3\perp} &= z_2 p_{5\perp} - p_{5\perp} \\
\Rightarrow p_{5\perp} &= \frac{q_{3\perp}}{z_2 - 1}
\end{aligned} \tag{154}$$

$$\begin{aligned}
q_{3\perp} &= p_{6\perp} + q_{4\perp} \\
q_{4\perp} &= z_3 p_{6\perp} - p_{6\perp} \\
\Rightarrow p_{6\perp} &= \frac{q_{4\perp}}{z_3 - 1}
\end{aligned} \tag{155}$$

We can eliminate $q_{3\perp}$ in expression for $p_{5\perp}$:

$$\begin{aligned}
p_{5\perp} &= \frac{p_{6\perp} z_3}{z_2 - 1} \\
\Rightarrow p_{5\perp} &= q_{4\perp} \frac{z_3}{(z_3 - 1)(z_2 - 1)}
\end{aligned} \tag{156}$$

It is necessary to compute the value $\frac{q_{1\perp}}{q_{4\perp}}$. We can use momentum conservation along the t-channel to write:

$$\begin{aligned}
q_{1\perp} &= p_{4\perp} + p_{5\perp} + p_{6\perp} + q_{4\perp} \\
\frac{q_{1\perp}}{q_{4\perp}} &= \frac{q_{1\perp}}{q_{4\perp}(1 + z_1)} + \frac{z_3}{(z_3 - 1)(z_2 - 1)} + \frac{1}{z_3 - 1} \\
\frac{q_{1\perp}}{q_{4\perp}} &= \frac{z_3 z_2 (1 + z_1)}{z_1 (z_3 - 1)(z_2 - 1)} \equiv \sigma \quad (\text{book-keeping})
\end{aligned} \tag{157}$$

It can also be shown:

$$\frac{q_{1\perp}}{q_{2\perp}} = (z_1 + 1)/z_1 \tag{158}$$

$$\frac{q_{1\perp}}{q_{3\perp}} = \frac{(1 + z_1)z_2}{z_1(-1 + z_2)} \tag{159}$$

$$q_{1\perp} q_{4\perp}^* = |q_{4\perp}| \sigma \tag{160}$$

$$q_{1\perp}^* q_{4\perp} = |q_{1\perp}|^2 \frac{1}{\sigma} \tag{161}$$

References

- ¹N. Zettili, *Quantum mechanics: concepts and applications* (Wiley, 2022).
- ²L. J. Dixon, “A Brief Introduction to Modern Amplitude Methods”, in *Journeys Through the Precision Frontier: Amplitudes for Colliders* (World Scientific) Chap. Chapter 2, pp. 39–97.
- ³G. Brumfiel, “LHC by the numbers”, [Nature](#), **10.1038/news.2008.1085** (2008).
- ⁴G. Altarelli and L. Di Lella, *Proton anti-proton collider physics* (WSP, Singapore, 1989).
- ⁵G. Chachamis, “BFKL phenomenology”, (2015).
- ⁶S. Weinzierl, *Tales of 1001 gluons*, 2016.
- ⁷J. R. Andersen and J. M. Smillie, “Multiple jets at the LHC with high energy jets”, [Journal of High Energy Physics](#) **2011**, **10.1007/jhep06(2011)010** (2011).
- ⁸V. S. Fadin, E. A. Kuraev, and L. N. Lipatov, “On the Pomeranchuk Singularity in Asymptotically Free Theories”, [Phys. Lett. B](#) **60**, 50–52 (1975).
- ⁹J. R. Forshaw and D. A. Ross, *Quantum chromodynamics and the pomeron*, Cambridge Lecture Notes in Physics (Cambridge University Press, 1997).
- ¹⁰V. Del Duca, *An introduction to the perturbative QCD pomeron and to jet physics at large rapidities*, 1995.
- ¹¹L. N. Lipatov, “Reggeization of the Vector Meson and the Vacuum Singularity in Non-abelian Gauge Theories”, *Sov. J. Nucl. Phys.* **23**, 338–345 (1976).
- ¹²E. A. Kuraev, L. N. Lipatov, and V. S. Fadin, “Multi - Reggeon Processes in the Yang-Mills Theory”, *Sov. Phys. JETP* **44**, 443–450 (1976).
- ¹³E. A. Kuraev, L. N. Lipatov, and V. S. Fadin, “The Pomeranchuk Singularity in Nonabelian Gauge Theories”, *Sov. Phys. JETP* **45**, 199–204 (1977).
- ¹⁴I. I. Balitsky and L. N. Lipatov, “The Pomeranchuk Singularity in Quantum Chromodynamics”, *Sov. J. Nucl. Phys.* **28**, 822–829 (1978).
- ¹⁵V. S. Fadin and L. N. Lipatov, “BFKL pomeron in the next-to-leading approximation”, [Phys. Lett. B](#) **429**, 127–134 (1998).
- ¹⁶M. Ciafaloni and G. Camici, “Energy scale(s) and next-to-leading BFKL equation”, [Phys. Lett. B](#) **430**, 349–354 (1998).
- ¹⁷A. V. Kotikov and L. N. Lipatov, “NLO corrections to the BFKL equation in QCD and in supersymmetric gauge theories”, [Nucl. Phys. B](#) **582**, 19–43 (2000).
- ¹⁸A. V. Kotikov and L. N. Lipatov, “DGLAP and BFKL equations in the $N = 4$ supersymmetric gauge theory”, [Nucl. Phys. B](#) **661**, [Erratum: *Nucl.Phys.B* 685, 405–407 (2004)], 19–61 (2003).
- ¹⁹V. Del Duca, R. Marzucca, and B. Verbeek, “The gluon Regge trajectory at three loops from planar Yang-Mills theory”, [Journal of High Energy Physics](#) **2022**, 149 (2022).

- ²⁰E. P. Byrne, V. D. Duca, L. J. Dixon, E. Gardi, and J. M. Smillie, “One-loop central-emission vertex for two gluons in $n=4$ super yang-mills theory”, [Journal of High Energy Physics](#) **2022**, [10.1007/jhep08\(2022\)271](#) (2022).
- ²¹C. N. Yang and R. L. Mills, “Conservation of isotopic spin and isotopic gauge invariance”, [Phys. Rev.](#) **96**, 191–195 (1954).
- ²²Vittorio Del Duca, *Scattering amplitudes in quantum field theories*, 2022.
- ²³H. Elvang and Y.-t. Huang, *Scattering Amplitudes in Gauge Theory and Gravity* (Cambridge University Press, 2015).
- ²⁴S. J. Parke and T. R. Taylor, “Amplitude for n -gluon scattering”, [Phys. Rev. Lett.](#) **56**, 2459–2460 (1986).
- ²⁵R. Britto, F. Cachazo, and B. Feng, “New recursion relations for tree amplitudes of gluons”, [Nuclear Physics B](#) **715**, 499–522 (2005).
- ²⁶Z. Bern, V. D. Duca, L. J. Dixon, and D. A. Kosower, “All non-maximally-helicity-violating one-loop seven-gluon amplitudes in $n = 4$ super-yang-mills theory”, [Physical Review D](#) **71**, [10.1103/physrevd.71.045006](#) (2005).
- ²⁷E. Levin, *Everything about reggeons. Part I: Reggeons in ”soft” interaction*, 1998.
- ²⁸D. Miller, *Determining the three-gluon Central-emission-Vertex at tree level: Mathematica files*, 2023.
- ²⁹A. van Hameren, “BCFW recursion for off-shell gluons”, [Journal of High Energy Physics](#) **2014**, 138 (2014).